symmetry

MDPI

Article

Algebraic DVR Approaches Applied to Piecewise Potentials: Symmetry and Degeneracy

Eduardo Suárez [1], Rubén Dario Santiago-Acosta [2] and Renato Lemus [1,*]

[1] Instituto de Ciencias Nucleares, UNAM A.P. 70-543, Circuito Exterior, C. U., Mexico City 04510, Mexico; easp_24@comunidad.unam.mx
[2] Tecnológico de Monterrey, Escuela de Ingeniería y Ciencias, Carr. al Lago de Guadalupe Km. 3.5, Monterrey 64849, Mexico; ruben.dario@tec.mx
* Correspondence: renato@nucleares.unam.mx

Abstract: Algebraic discrete variable representation (DVR) methods that have been recently proposed are applied to describe 1D and 2D piecewise potentials. First, it is shown that it is possible to use a DVR approach to describe 1D square well potentials testing the wave functions with exact results. Thereafter, Morse and Pöschl-Teller (PT) potentials are described with multistep piecewise potentials in order to explore the sensibility of the potential to reproduce the transition from a pure square well energy pattern to an anharmonic energy spectrum. Once the properties of the different algebraic DVR approaches are identified, the 2D square potential as a function of the potential depth is studied. We show that this system displays natural degeneracy, accidental degeneracy and systematic accidental degeneracy. The latter appears only for a confined potential, where the symmetry group is identified and irreducible representations are constructed. One particle confined in a rectangular well potential with commensurate sides is also analyzed. It is proved that the systematic accidental degeneracy appearing in this system is removed for finite potential depth.

Keywords: algebraic DVR method; piecewise potentials; natural degeneracy; accidental degeneracy; systematic accidental degeneracy

Citation: Suárez, E.; Santiago-Acosta, R.D.; Lemus, R. Algebraic DVR Approaches Applied to Piecewise Potentials: Symmetry and Degeneracy. *Symmetry* **2022**, *14*, 445. https://doi.org/10.3390/sym14030445

Academic Editors: Enrico Bodo and Sergei D. Odintsov

Received: 19 December 2021
Accepted: 16 February 2022
Published: 23 February 2022

1. Introduction

The quantum box, also known as the 1D infinite square well, is the simplest quantum mechanical system used in textbooks to exemplify the solution of the Schrödinger equation. This system has only bound states and its generalization to 2D and 3D Cartesian infinite square well potentials is straightforward [1–4]. Although the energy spectra are indeed easy to obtain, the 2D and 3D cases present a degeneracy pattern not explained by the geometrical point group associated with square and cubic geometrical symmetries; the degeneracy degree is expected to correspond to the dimension of one of the irreducible representations (irrep) of the symmetry group. In situations where the latter is not fulfilled, degeneracy is identified as accidental. However the appearance of systematic accidental degeneracy signals the presence of hidden symmetries, a fact that always deserves further physical insight [5]. In such cases, a new symmetry group is expected to exist where the accidental degeneracy is rendered normal. The non-relativistic hydrogen atom is representative of this situation where the $SO(3)$ geometrical symmetry should be extended to a four-dimensional $SO(4)$ group, in which its generators correspond to angular momentum and Runge–Lenz components [6–8]. Surprisingly, the considerably more simple system of one particle in an impenetrable 2D square box presents a similar situation where the geometrical symmetry group $\mathcal{C}_{4v}$ had to be extended to the semidirect group $\mathcal{G} = \mathcal{T} \wedge \mathcal{C}_{4v}$, where $\mathcal{T}$ is a one-dimensional compact continuous group [9]. The fact that this group contains discrete as well as continuum elements makes the construction of its irreps a non trivial task, which from a formal point of view has a close analogy with the construction of irreps for space groups [10]. A similar situation is present for the case of a cubic box,

where the extended group turns out to be $\mathcal{G} = \mathcal{T} \wedge \mathcal{O}_h$, where $\mathcal{T}$ is a two dimensional compact continuous group for which generators correspond to linear combinations of one-dimensional Hamiltonians [11].

An interesting situation emerges when the potential depth becomes finite either for the square or cubic well potentials. In this study, we shall prove that, in the high region of the spectrum , degenerate levels split to render normal degeneracy with respect to the geometrical symmetry group, albeit with the possibility of remaining an accidental degeneracy as energy decreases. Hence, the symmetry group becomes the expected geometrical group $\mathcal{C}_{4v}$ or $\mathcal{O}_h$ for the square and cubic potentials, respectively, although with possible presence of accidental degeneracy, which is completely removed by enough decreases in the potential depth. This behavior is also present for a particle in an impenetrable rectangular well potential with commensurate sides [12].

Although analyses of the square, rectangular and cubic impenetrable well potentials have been presented in a more or less degree of formality [9,11,12], their study for finite wells has not been worked out. One of the reasons for this may be that the solutions cannot be obtained in a straightforward manner but also because their study requires the use of the machinery of group representation theory, a background beyond the scope of standard textbooks. In contrast, 1D piecewise constant potentials do not present degeneracy for the bound states, an ideal situation to simplify the analytic manipulations for illuminating features of both the postulates and properties of eigenfunctions; the study of piecewise potentials provides the background to estimate, in a qualitative form, the behavior of wave functions for arbitrary potentials. In particular, a half-square well potential, symmetric square well and the delta function potentials provide common systems in textbooks to illustrate the concepts of quantum mechanic. Even though the general solutions in each region of the potential are easily obtained, the eigenvalues are determined only by solving transcendental equations after imposing the matching conditions in wave functions and derivatives. When the piecewise potential presents two or three regions, this approach is feasible, but as regions increases, the procedure become somewhat cumbersome in 1D systems, but much worse in 2D and 3D potentials. Hence, alternative approaches that avoid the explicit matching of the wave functions and their derivatives are welcome.

A powerful method that allows the solutions of piecewise potentials to be obtained is the discrete variable representation approach (DVR). The feature of this approach is that it provides a discrete basis where the coordinate is diagonal and, consequently, the representation of the potential too. The DVR method has a long story, with original ideas proposed in the 1960s [13,14] and becoming widely used in the 1980s with the works of J.C. Light and others [15–23]. However, this method has been independently developed with different names: quadrature discretization method [24–29], Lagrange mesh method [30–33] and configuration localized states [34–36]. The main ingredient of these methods is the use of orthonormal polynomials with the Gaussian quadrature method to establish a grid associated with the zeros of the polynomials. The common features and differences between the DVR methods are provided by Baye [33]. The fundamentals of the DVR methods can be identified in 1D systems, but its extension to higher dimensions was immediate. However it is convenient to highlight two routes to extend the method to higher dimensions. One possibility consists in considering systems that intrinsically are defined in 3D, such as the solution of the non-relativistic hydrogen atom. Another possibility for proceeding to higher dimensions consists in taking direct products of 1D systems. This situation is present in the description of the vibrational degrees of freedom where for each internal coordinate an oscillator is associated [37], although the direct product has also been employed to determine ro-vibrational spectra [38]. The direct product basis has the advantage of simplicity, but it has the disadvantage of the large basis dimension to obtain converged energy levels. It is possible to overcome this problem at least in part by the use of the Lanczos algorithm, which does not require storage of the Hamiltonian matrix [39,40], a method that combined with a procedure to exclude functions that do not significantly contribute to the physical description allows the computational cost to be reduced [41].

Recently, an alternative DVR method based on dynamical groups $U(n+1)$ for nD systems was proposed. These groups emerge when the number of bosons $\hat{n}$ associated with the harmonic oscillator is constrained by introducing an extra scalar boson $s^\dagger(s)$, imposing a constant total of number of bosons $\hat{N} = \hat{n} + s^\dagger s$ [42]. In this manner, number N characterizes the Hilbert space where the physical description is carried out. This scheme to construct a dynamical group has two advantages; on one hand, the dynamical group is identified with a compact unitary group and, on the other hand, three physical group chains are identified. The key to derive a DVR method relies on the connection of the $U(n+1)$ algebraic scheme with the configuration space in the N large limit. This connection leads us to associate the $U(n)$ chain with energy representation, the $SO(n+1)$ chain with coordinate representation and the $\overline{SO}(n+1)$ chain with momentum representation. The diagonalization of the coordinate and momentum in the $U(n)$ basis provides bases where the coordinate and momentum are diagonal. In this scheme, it is through the transformation brackets connecting the different bases that makes it possible to obtain the representation of the Hamiltonian matrix in a simple form in terms of diagonal matrices, a feature characterizing a DVR approach. This approach has been called the unitary group approach (UGA), and it has been presented in detail for nD potentials [43–48]. A natural alternative to this approach consists in projecting the harmonic oscillator basis to a subspace of finite dimension. The discrete variable representation —called the HO-DVR approach due to the fact that it is purely defined in the space of Harmonic oscillator wave functions— is obtained through the diagonalization of the algebraic representation of operators r^2 and p^2. The resulting discrete basis exactly corresponds to localized states related with the zeros of the polynomials associated with the solutions of the harmonic oscillator. Both the $U(n+1)$-UGA and HO-DVR methods are defined in terms of the harmonic oscillator basis, but they provide different discrete representation bases and consequently one method may be more suitable for a specific problem [49]. In fact, in the description of the Stark effect in the non-relativistic Hydrogen atom, $U(4)$-UGA turns out to be more suitable for describing the breaking of spherical symmetry due to the electric field [50], while in all tested potentials where the angular momentum is conserved, HO-DVR offers better convergence [49].

Although the Harmonic oscillator basis has proved to be useful in applications from atoms to quarks [51], it is not expected to be suitable for any potential. A basis to be used in a given problem depends on the boundary conditions and, consequently, the alternative algebraic DVR methods associated with different bases are needed in order to improve convergence. In this venue, two more algebraic DVR approaches for 1D systems have been proposed, one associated with the Morse potential (M-DVR) and the other one to the Pöschl-Teller potential (PT-DVR), both based on the realization of the coordinate and momentum in terms of the generators of the $U(1,1)$ dynamical group [49]. As expected, the M-DVR approach is more appropriate for asymmetric potentials while the PT-DVR method represents an improvement to symmetric potentials where bound and continuous energies are present. These methods, although constrained to 1D systems, provide useful bases to deal with multidimensional problems such as nD square well potentials with finite wells.

In this contribution, we present a study of one particle under 1D and 2D piecewise potentials. This work has two goals. First, we are interested in studying convergence in these kind of systems. This is a nontrivial question given the fact that potentials that are not analytic do not provide exponential convergence [52]. On the other hand, the algebraic DVR approach provide us with a simple and powerful method to study symmetry breaking $\mathcal{T} \wedge \mathcal{C}_{4v} \downarrow \mathcal{C}_{4v}$ appearing when the walls of a confined particle in a 2D square well potential become finite. We intend to show that this simple system exemplifies the concepts of natural, accidental and systematic accidental degeneracy, which constitute fundamental concepts in establishing a connection between symmetry and degeneracy. In addition, we present the study of a particle confined in a rectangular well potential with commensurate sides, a system where a systematic accidental degeneracy also appears, and it is removed when the depth of the potential becomes finite.

This article is organized as follows. Section 2 is devoted to presenting the salient features of 1D-DVR approaches to be used in the description of piecewise potentials, presenting as an example the HO-DVR approach based on the harmonic oscillator basis. Alternative methods are provided in the Appendix A. In Section 3, the analysis of convergence for a symmetric and asymmetric well potentials using the different 1D algebraic DVR approaches is presented. In the same section, the transition from the spectrum characterizing the square well potentials to an anharmonic spectrum provided by PT and Morse potentials is also analyzed. In Section 4, the analysis of the energy spectrum for square well potential as a function of the potential depth in terms of the direct product of 1D systems is presented. Section 5 is devoted to presenting a similar analysis for a particle in a rectangular well potential with commensurate sides. Finally, in Section 6, the summary and our conclusions are presented.

2. Algebraic DVR Methods in 1D Systems

The aim of this section is to provide the basic ingredients characterizing algebraic DVR methods that will be applied to obtain the solutions of systems defined in terms of piecewise potentials. We shall take as an example the HO-DVR method. Additional methods known as PT-DVR, M-DVR and $SU(2)$-UGA are presented in the Appendix A. The basic idea of these methods consists in diagonalizing the matrix representation of the coordinate and momentum to generate discrete variable representation bases, which allows the matrix representation of the Hamiltonian to be expressed in terms of diagonal matrices for both kinetic and potential terms. The relevant aspect of this approach is that the matrix elements are obtained with purely algebraic means, avoiding the intrinsic numerical problems of integration.

The 1D harmonic oscillator with reduced mass μ and frequency ω is defined through the following Hamiltonian:

$$\hat{H}^{\text{h.o.}} = \frac{1}{2\mu}p^2 + \frac{\omega^2\mu}{2}\,q^2, \tag{1}$$

with eigenfunctions given by the following [1]:

$$\psi_n(q) = N_n\, e^{-\frac{q^2}{2\lambda_0^2}}\, H_n(q/\lambda_0), \tag{2}$$

where $H_n(x)$ stands for Hermite polynomials, with $\lambda_0 = \sqrt{\hbar/(\omega\mu)}$ and normalization constant $N_n = (n!2^n\lambda_0\sqrt{\pi})^{-1/2}$. Introducing the bosonic operators $\{a^\dagger, a\}$ with the usual realization:

$$a^\dagger = \frac{1}{\sqrt{2}}\left(\frac{1}{\lambda_0}q - i\frac{\lambda_0}{\hbar}p\right); \qquad a = \frac{1}{\sqrt{2}}\left(\frac{1}{\lambda_0}q + i\frac{\lambda_0}{\hbar}p\right), \tag{3}$$

the Hamiltonian takes the following simple form:

$$\hat{H}^{\text{h.o.}}_{\text{Fock}} = \hbar\omega(\hat{n} + 1/2); \quad \hat{n} = a^\dagger a, \tag{4}$$

with eigenkets [1]

$$|n\rangle = \frac{1}{\sqrt{n!}}\,(a^\dagger)^n|0\rangle. \tag{5}$$

Using this algebraic representation, the matrix elements for the coordinate and momenta are easily obtained

$$\langle n'|q|n\rangle = \frac{\lambda_0}{\sqrt{2}}\left(\sqrt{n+1}\,\delta_{n',n+1} + \sqrt{n}\,\delta_{n',n-1}\right), \tag{6}$$

$$\langle n'|p|n\rangle = \frac{i}{\sqrt{2}}\frac{\hbar}{\lambda_0}\left(\sqrt{n+1}\,\delta_{n',n+1} - \sqrt{n}\,\delta_{n',n-1}\right). \tag{7}$$

If we now consider the projection to a finite space of the following:

$$\mathcal{L}_N^{\text{h.o.}} = \{|n\rangle, n = 0, 1, \ldots, N-1\}, \tag{8}$$

and carry out their diagonalization, we obtain the discrete representation of the coordinate and momenta given by the following eigenvectors:

$$|q_i\rangle = \sum_{n=0}^{N-1} \langle n|q_i\rangle |n\rangle, \tag{9}$$

$$|p_i\rangle = \sum_{n=0}^{N-1} \langle n|p_i\rangle |n\rangle, \tag{10}$$

where matrices $\mathbf{T} = ||\langle n|q_i\rangle||$ and $\mathbf{W} = ||\langle n|p_i\rangle||$ correspond to the coefficients that define the basis transformations (9) and (10) where coordinates and momentum are diagonal.

$$q|q_i\rangle = q_i|q_i\rangle, \qquad p|p_i\rangle = p_i|p_i\rangle. \tag{11}$$

Equation (11) establishes the discrete variable representation characterized by the following:

$$\langle q_j|V(q)|q_i\rangle = V(q_i)\delta_{i,j}, \qquad \langle p_j|G(p)|p_i\rangle = G(p_i)\delta_{i,j} \tag{12}$$

for any function of either coordinates $V(q)$ or momentum $G(p)$. The matrix representation of a Hamiltonian associated with a general potential $V(q)$ in the harmonic oscillator basis thus takes the following form:

$$\mathbf{H} = \mathbf{W}^\dagger \mathbf{\Lambda}^{(p)} \mathbf{W} + \mathbf{T}^\dagger \mathbf{\Lambda}^{(q)} \mathbf{T}, \tag{13}$$

where the diagonal matrices are given by $||\mathbf{\Lambda}^{(p)}|| = (p_i^2/2\mu)\delta_{ij}$ and $||\mathbf{\Lambda}^{(q)}|| = V(q_i)\delta_{ij}$ in momentum and coordinate representations, respectively. In Appendix A, alternative methods following the same idea are presented.

3. 1D Square Well Potentials

Here, we start considering a particle with mass μ inside a symmetric square well potential defined as follows:

$$V(x) = \begin{cases} 0 \quad ; & x \in [-a/2, a/2] \\ V_0 \quad ; & x > a/2, \quad x < -a/2, \end{cases} \tag{14}$$

and depicted in Figure 1. Because of the invariance of the potential under inversion, the solutions are expected to have good parity. Following the usual procedure of imposing the boundary matching relations of both continuity and derivatives for the functions at the limits of the regions, we have the following for the even functions:

$$\begin{aligned} \Psi_I^e(x) &= Ae^{\alpha x}, \\ \Psi_{II}^e(x) &= Ae^{-\alpha a/2} \sec(ka/2) \cos(kx), \\ \Psi_{III}^e(x) &= Ae^{-\alpha x}, \end{aligned}$$

with the definitions $\alpha^2 = 2\mu E/\hbar^2$ and $k^2 = 2\mu V_o/\hbar^2 - \alpha^2$. The energies are obtained by the following transcendental equation.

$$\tan(ka/2) = \alpha/k. \tag{15}$$

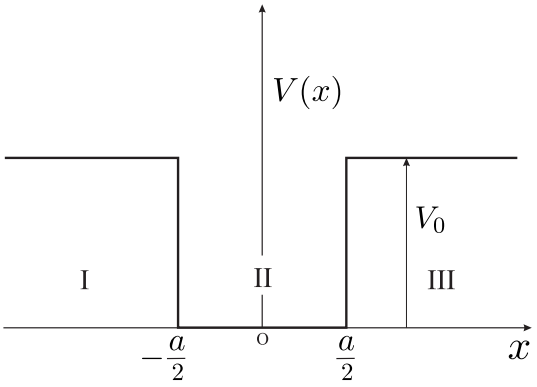

Figure 1. Symmetric square well potential. The origin was chosen in order to obtain wave functions with good parity.

On the other hand, for the odd functions, we have the following:

$$\begin{aligned}\Psi_I^o(x) &= Ae^{\alpha x},\\ \Psi_{II}^o(x) &= -Ae^{-\alpha a/2}\csc(ka/2)\sin(kx),\\ \Psi_{III}^o(x) &= -Ae^{-\alpha x},\end{aligned}$$

with the corresponding transcendental equation for energies

$$\tan(ka/2) = -k/\alpha. \tag{16}$$

In both cases, amplitude A is determined by normalization. A particular case of academic interest is the confined particle corresponding to infinite potential barriers. In this case, the eigenvalues take the following form:

$$E_n = \frac{\hbar^2\pi^2}{2\mu a^2}n^2, \tag{17}$$

with eigenfunctions carrying good parity:

$$\Psi_n^{(e)}(x) = \sqrt{\frac{2}{a}}\cos\left(\frac{n\pi}{a}x\right); \quad n = 1,3,5,\ldots \tag{18}$$

$$\Psi_n^{(o)}(x) = \sqrt{\frac{2}{a}}\sin\left(\frac{n\pi}{a}x\right); \quad n = 2,4,6,\ldots \tag{19}$$

for even and odd parity, respectively.

The procedure to obtain the solutions for the potential (14), although relatively easy to obtain, has two inconveniences: On one hand, energies are obtained by transcendental equations and, on the other hand, this approach becomes very cumbersome when additional piecewise steps in the potential are involved. We now proceed to obtain the bound states of potential (14) using algebraic DVR approaches presented in Appendix A. Because of the symmetry of the potential, the appropriate methods satisfying the boundary conditions of potential (14) are the HO-DVR, PT-DVR and $SU(2)$-UGA approaches. The Hamiltonian matrix representation in HO-DVR and $SU(2)$-UGA-DVR approaches takes the general form:

$$\mathbf{H} = \mathbf{\Lambda}^{(E)} + \mathbf{T}^\dagger\mathbf{\Lambda}^{(q)}\mathbf{T}, \tag{20}$$

where $\mathbf{\Lambda}^{(E)}$ is the diagonal contribution of the harmonic oscillator contribution with an explicit expression depending on the method in the following form:

$$\text{HO-DVR}: \quad ||\mathbf{\Lambda}^{(E)}|| = \hbar\omega\left[n+\frac{1}{2}\right]\delta_{nn'}, \tag{21}$$

$$U(2)-UGA: \quad ||\mathbf{\Lambda}^{(E)}|| = \hbar\omega\left[n+\frac{1}{2}-\epsilon\frac{n^2}{N}\right]\delta_{nn'}, \tag{22}$$

where $\epsilon = 1$ for $n < N/2$ and $\epsilon = 0$ for $n \geq N/2$ in accordance with (A36). The diagonal matrix $\mathbf{\Lambda}^{(q)}$ corresponds to the modified potential in the coordinate representation given by the following.

$$\text{HO-DVR}: \quad ||\mathbf{\Lambda}^{(q)}|| = \hbar\omega\left[V(x_i)-\frac{1}{2}\mu\omega^2 q_i^2\right]\delta_{ij}, \tag{23}$$

$$U(2)\text{-UGA}: \quad ||\mathbf{\Lambda}^{(q)}|| = \hbar\omega\left[V\left(\zeta\sqrt{\frac{2}{N}}\right)-\frac{1}{N}\mu\omega^2\zeta^2\right]\delta_{\zeta\zeta'}. \tag{24}$$

Accordingly the transformation coefficients involved in (20) are defined as follows.

$$\text{HO-DVR}: \quad \mathbf{T} = ||\langle n|q_i\rangle||; \quad \textit{Equation (9)} \tag{25}$$

$$U(2)\text{-UGA}: \quad \mathbf{T} = ||\langle [N]n|[N]\zeta\rangle||; \quad \textit{Equation (A34)}. \tag{26}$$

Regarding the PT-DVR method, the Hamiltonian matrix representation takes the form (13), where we have for the diagonal matrix $\mathbf{\Lambda}^{(p)}$ in the momentum representation, $||\mathbf{\Lambda}^{(p)}|| = \frac{p_i^2}{2\mu}\delta_{ij}$, while for the diagonal matrix for the potential in the position representation, we have $||\mathbf{\Lambda}^{(q)}|| = V(q_i)\delta_{ij}$. In this case, both transformation coefficients defined in (A15) are needed. In every case, the potential in discretized representation $V(x_i)$ corresponds to the square well potential defined in (14). Diagonalization is carried out in a truncated basis specified by N, the dimension of the finite projected space. Each dimension space provides a particular set of discretized points that are distributed along the piecewise potential in an inhomogeneous form. This feature does not allows a smooth convergence, as we shall see.

In order to test the methods, we start the application of DVR methods to the square well potential with infinite walls, which in practice were taken to have a height of $V_0 = 10^8$ cm^{-1} with the length of the box at $a = 4$ Å. In all cases of this contribution, the mass was taken to be $\mu = 1.6726219 \times 10^{-27}$ kg, an approximation to the proton mass. The comparisons between the spectrum generated by the three approaches (HO-DVR, PT-DVR and $SU(2)$-UGA) and the exact energies are displayed in Table 1. The criterion to obtain convergence in energies for HO-DVR and PT-DVR methods was to reach less than 1 % of errors in all states. Both methods are similar in both quality and basis dimension. However, $SU(2)$-UGA does not provide reasonable results even when considering a much larger basis of $N = 2483$. Increasing the basis dimension does not result in a stable calculation, albeit the chosen basis dimension corresponds to a minimum in the rms. Since $SU(2)$-UGA provides a discretized basis but is not localized, these results mean that localized discrete bases are indeed the best option to describe piecewise potentials.

We now consider the case of a 1D square well potential with finite potential $V_0 = 1000$ cm^{-1} and length $a = 4$ Å. This system presents 10 bound states that can be obtained in exact form by solving transcendental Equations (15) and (16). The comparisons between the exact energies and the ones obtained using DVR methods are provided in Table 2. As expected, for $SU(2)$-UGA, a much larger basis is needed to obtain comparable errors. In contrast, the HO-DVR and PT-DVR approaches provide a pretty good description of the system. The criterion to obtain convergence in the energies for both HO-DVR and PT-DVR methods was again to reach less than 1 % of error in all states. In order to obtain a more detailed comparison between the HO-DVR and PT-DVR methods, in Figure 2, a plot

of the errors is depicted. This shows that the PT-DVR approach provides a better uniform description in most of the states. Only in the last state was the error observed to increase over the error provided by the HO-DVR approach.

Table 1. Description of the 1D potential well with infinite walls with the algebraic DVR methods: HO-DVR, PT-DVR and $SU(2)$-UGA. The parameters for the potential were taken to be $a = 4$ Å and $V_0 = 10^8$ cm^{-1}, with $\mu = 1.6726219 \times 10^{-27}$ kg. In addition, the fitted parameters associated with the algebraic DVR methods were found to be $\omega = 2.0 \times 10^{13}$ s^{-1}, $\alpha = 4.5 \times 10^9$ m^{-1} and $\omega = 1.6 \times 10^{12}$ s^{-1} for HO-DVR, PT-DVR and $SU(2)$-UGA, respectively. In each case, E_c is the calculated energy in cm^{-1}. The zero of the energy was taken to be at the bottom of the well. The basis dimension N needed to obtain the displayed description was also included.

		HO-DVR $N = 58$		**PT-DVR** $N = 60$		**SU(2)-UGA** $N = 2483$	
n	**Exact**	E_c(cm^{-1})	**% Error**	E_c(cm^{-1})	**% Error**	E_c(cm^{-1})	**% Error**
1	10.32	10.37	0.45	10.32	0.04	18.73	81.41
2	41.30	41.37	0.16	41.16	0.33	49.35	19.50
3	92.92	93.34	0.45	92.88	0.04	100.13	7.76
4	165.19	165.43	0.14	164.62	0.35	170.66	3.31
5	258.11	259.30	0.46	258.02	0.03	260.43	0.90
6	371.67	372.05	0.10	370.28	0.37	368.68	0.80
7	505.89	508.31	0.48	505.75	0.03	494.70	2.21
8	660.75	660.80	0.01	657.97	0.42	637.34	3.54
9	836.26	840.45	0.50	836.11	0.02	795.73	4.85
10	1032.43	1030.30	0.21	1027.25	0.50	968.36	6.21

Table 2. Description of the 1D potential well using algebraic DVR methods: HO-DVR, PT-DVR and $SU(2)$-UGA. The parameters for the potential were taken to be $a = 4$ Å and $V_0 = 1000$ cm^{-1}. In this case the fitted parameters associated with the algebraic DVR methods were the same as in the previous case. The zero of the energy was located at the bottom of the well. The basis dimension N needed to obtained the displayed description was also included.

		HO-DVR $N = 58$		**PT-DVR** $N = 94$		**SU(2)-UGA** $N = 2483$	
n	**Exact**	E_c(cm^{-1})	**% Error**	E_c(cm^{-1})	**% Error**	E_c(cm^{-1})	**% Error**
1	9.11	9.02	0.99	9.07	0.44	17.79	95.28
2	36.43	36.07	0.99	36.25	0.49	45.58	25.12
3	81.83	81.13	0.86	81.51	0.39	91.64	11.99
4	145.27	144.03	0.85	144.69	0.40	155.55	7.08
5	226.53	224.90	0.72	225.76	0.34	236.75	4.51
6	325.34	323.16	0.67	324.26	0.33	334.44	2.80
7	441.25	439.07	0.49	440.13	0.25	447.65	1.45
8	573.49	571.19	0.40	572.19	0.23	575.08	0.28
9	720.62	719.82	0.11	719.86	0.11	714.90	0.79
10	878.85	878.85	0.00	878.18	0.08	863.81	1.71

Convergence in energy does not imply convergence in wave functions. Wave functions are tested with fidelity. Fidelity $F_\alpha(N)$ for a given state $|\Psi_\alpha\rangle$ parameterized with the basis dimension N is defined as the overlap between consecutive eigenstates separated by ΔN:

$$F_\alpha(N) = \langle \Psi_\alpha^{N+\Delta N} | \Psi_\alpha^N \rangle. \tag{27}$$

For the basis dimension given in Table 2, we have calculated the fidelity for each state taking $\Delta N = 20$. The results are displayed in Figure 3. The better quality of the

wave functions provided by the PT-DVR methods is manifested in the closer values to unity. In order to show the impact of fidelity on the quality of the wave functions, we display in Figure 4 the calculation of wave functions $\langle q|\Psi_1\rangle$, $\langle q|\Psi_5\rangle$ and $\langle q|\Psi_{10}\rangle$ provided by both methods, indicating fidelity. In order to identify the best approach, at the right of the wave functions, the absolute value of the difference between the exact and calculated wave function is also shown. From these results, it is clear that PT-DVR provides a better description in both energies and wave functions. This is a somewhat expected result, given the fact that the PT basis carries information about the continuum. From these results, it is clear that PT-DVR provides a better description in both energies and wave functions.

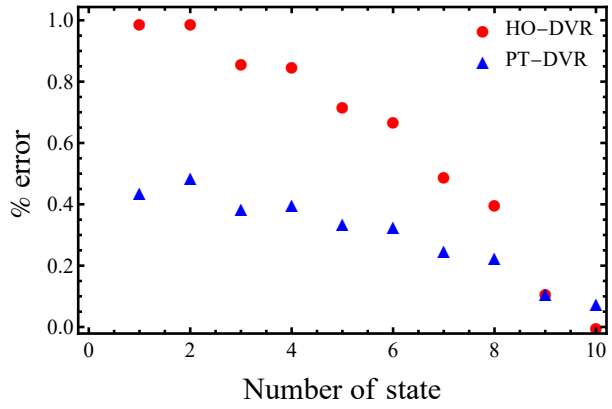

Figure 2. Comparison between the errors associated with the HO-DVR (solid circles) and PT-DVR (triangles) methods in accordance with the results provided in Table 2.

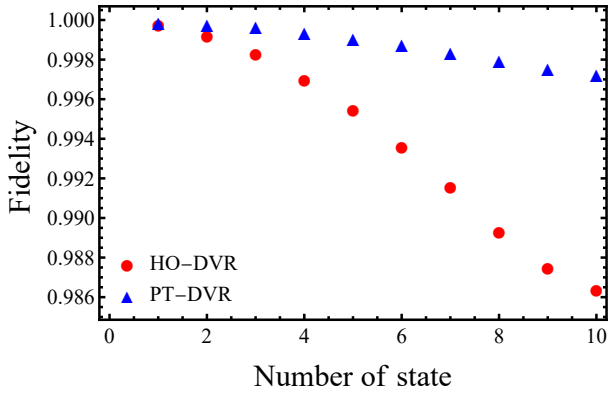

Figure 3. Fidelity obtained for each state displayed in Table 2 taking a step of $\Delta = 20$. The solid circles correspond to the HO-DVR method while the triangles stand for the PT-DVR approach.

One feature of this system is the peculiar N-dependence of convergence. In Figure 5, we present as an example the error dependence of basis dimension N for state $|\Psi_5\rangle$. The oscillations become evident as well as the fact that each method displays a characteristic pattern. We thus have to be careful in selecting the appropriate dimension N: it may be the case that increasing the basis does not imply a better convergence since, in these systems, an exponential convergence is not present [52], and a DVR method does not imply an variational approach [53]. Hence, in order to take full advantage of the DVR methods, a study of the errors should be conducted. It is only through this analysis that N can be appropriately chosen to obtain the best description.

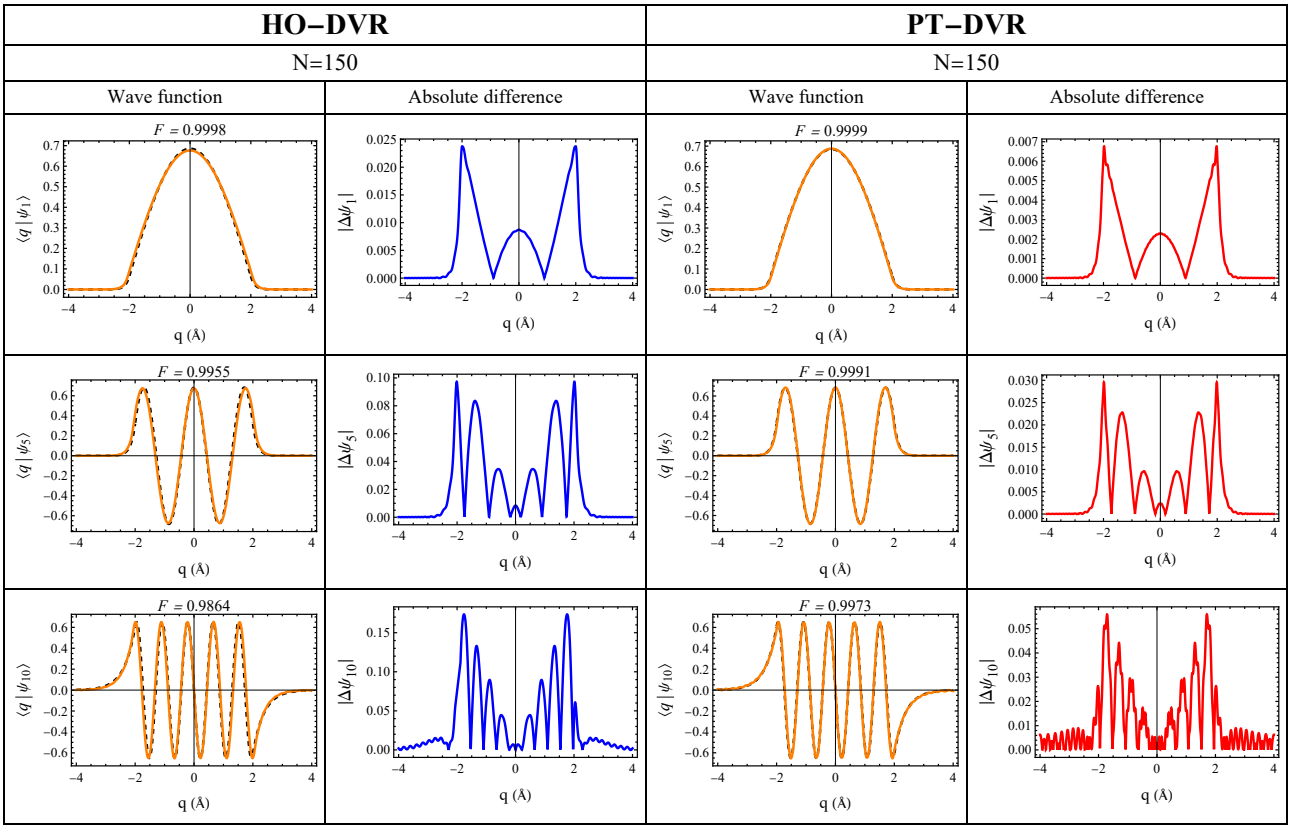

Figure 4. Particular wave functions provided by the HO-DVR and PT-DVR approaches taking equal basis dimension. The dashed lines correspond to the analytic wave functions. Values of the fidelity are included. At the right of the wave functions, the absolute value of the difference between the calculated and exact wave functions are also shown, reflecting a better description for PT-DVR.

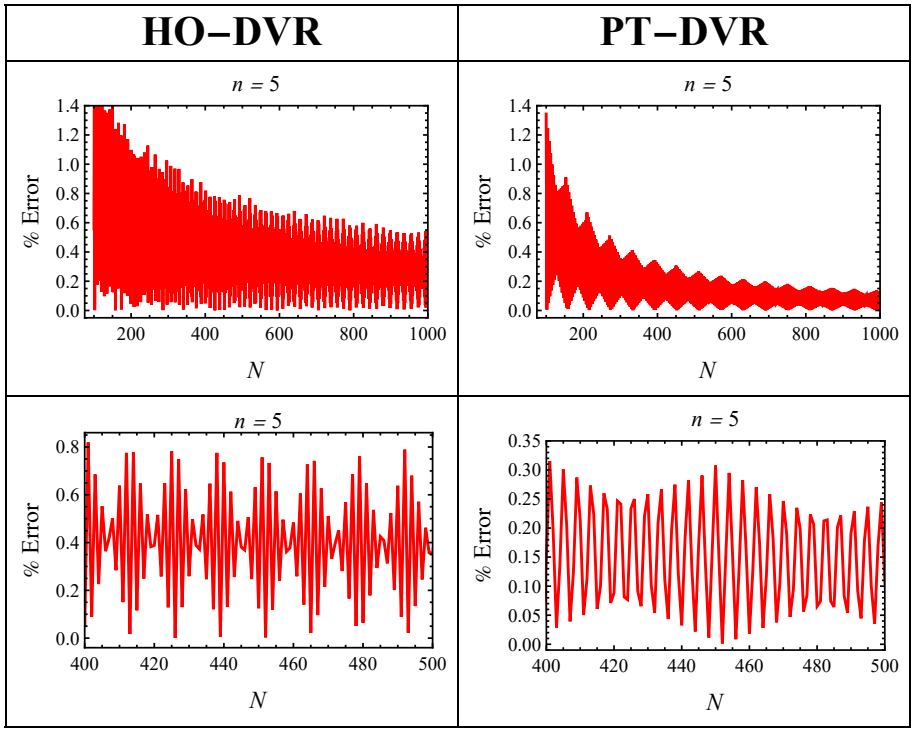

Figure 5. Errors associated with bound state $\langle q|\Psi_5\rangle$ as a function of basis dimension N. The second row corresponds to a zoom of the results given in the first row.

Multistep Piecewise Potentials

The potential displayed in Figure 1 may be compared with a realistic PT-potential. In a similar manner, the half-space square well potential may be compared with the Morse potential, as shown in Figure 6. This comparison is based on the same boundary conditions as well as the presence of continuum states. However, the corresponding spectra are completely different: While PT and Morse potentials have an anharmonic spectrum characterized by a negative slope in a Birge–Sponer plot involving difference $E_{v+1} - E_v = \hbar\omega_e - 2x_e\omega_e(v+1)$ vs. number of state, the square well potentials present a positive slope α in $E_{n+1} - E_n = \alpha(2n+1)$. This fact results in the conclusion that anharmonicity is not only a consequence of the presence of the continuum but is fundamental result of the form of the potential curve in particular regions. In order to elucidate the region of the potential responsable to the anharmonic behavior, we propose to represent both the PT and Morse potentials in terms of multipiecewise potentials, as displayed in Figure 7, where in the limit of infinite steps, true potentials are expected to be recovered. Our goal is to use the DVR approach to study the number of steps (degree of smoothness) to reproduce the anharmonicity pattern characterizing the molecular spectra.

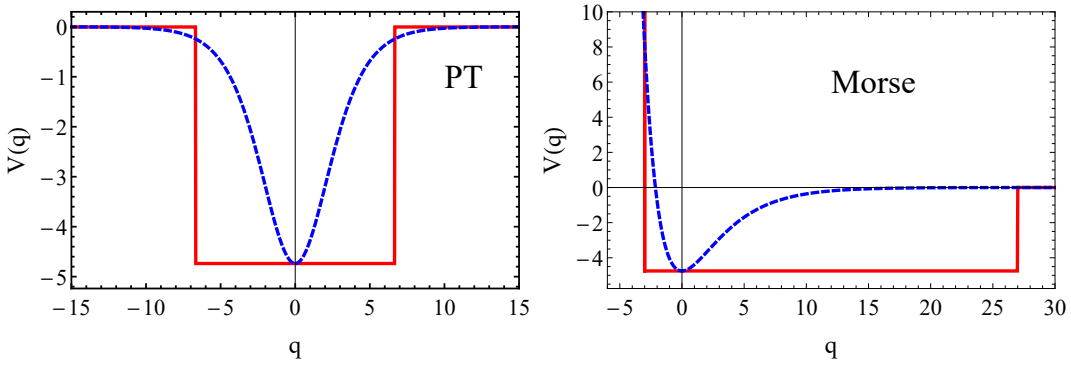

Figure 6. Comparison between the PT (**left** plot) and Morse (**right** plot) potentials with the simplest approximation in terms of piecewise potentials.

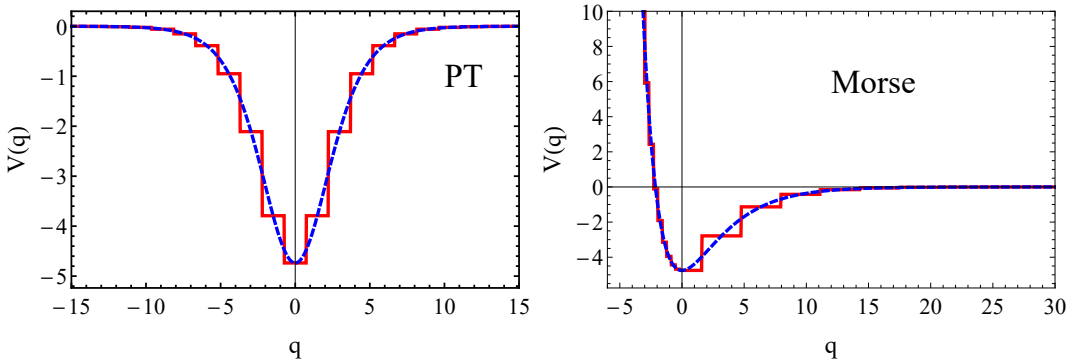

Figure 7. Representation of the PT and Morse potentials in terms of multistep-piecewise potentials.

First, we consider the PT potential approximated by a piecewise potential following the potential curve. We have divided the range of the potential in equals steps, a partition that implies a better approximation for the potential near the continuum. In Figure 8, the energy correlation as a function of the number of steps using both HO-DVR and PT-DVR methods is displayed. In these plots, the left limit corresponds to the exact energy spectrum for the square well potential, while the right limit corresponds to the exact PT spectrum. The first feature we notice is that the anharmonic energy pattern is reached with relatively few steps. As a consequence the anharmonic spectrum is determined by the form of the potential near the continuum. This analysis resembles the notch test used to establish the confident limits of different regions of the potential [48].

Although the general correlation pattern displayed in Figure 8 by both methods is the same, there are some subtle differences concerned with the smoothness of the oscillations associated with the convergence previously discussed and depicted in Figure 5. Beyond this subtle differences, it is clear that there is an advantage of the PT-DVR approach over the HO-DVR method.

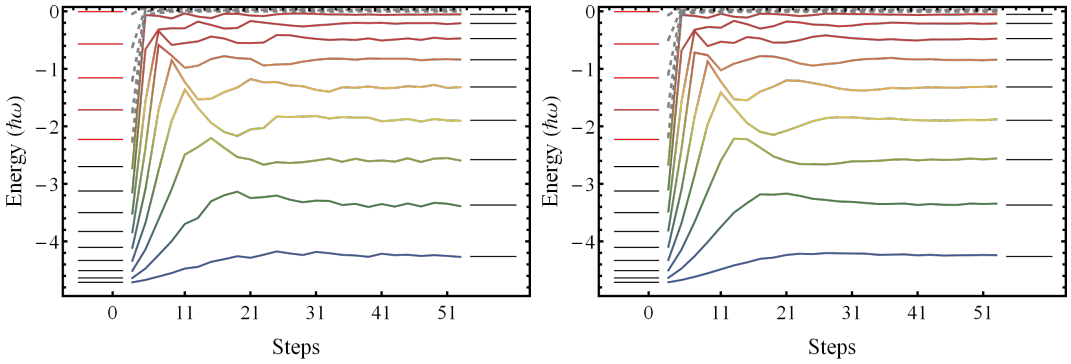

Figure 8. Correlation diagrams between the spectrum generated by the square well potential depicted in Figure 6 and the exact PT-potential as a function of the number of steps using the HO-DVR method (**left** figure) and the PT-DVR approach (**right** figure). In both cases, the basis dimension was taken to be $N = 230$. The levels with gray color correspond to states in the square well potential that move to the continuum region as the number of steps are increased.

We have also carried out the corresponding analysis by approximating the Morse potential with a piecewise potential using the M-DVR approach. The corresponding energy correlation diagram is displayed in Figure 9. Again, the anharmonic pattern is reached with relatively few steps due to the fact that the approximation displayed in Figure 7 implies a better approximation near the continuum. It is worth stressing the fact that the description of the bound states for the half-space square well potential strongly depends on the basis dimension. In order to show this dependence, we present two diagrams corresponding to $N = 150$ and $N = 2500$, respectively, where in the latter case the best description of the half-space square well potential becomes. The number of bound states for the half-space square well potential is much greater that the corresponding Morse spectrum. As the number of steps increases to approximate the Morse potential, most of the bound states move to the discretization description of the continuum.

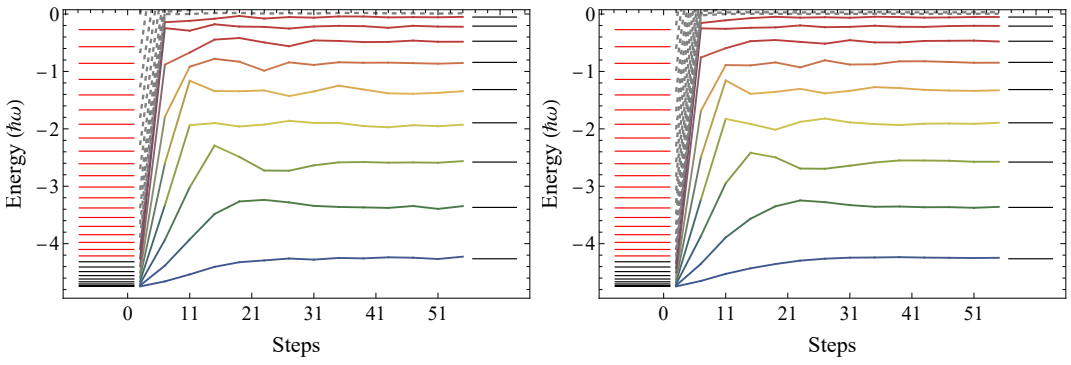

Figure 9. Correlation diagram between the spectrum generated by the half-space square well potential and the Morse potential as a function of the number of steps using the Morse-DVR approach. The **left** figure corresponds to the analysis using a basis dimension $N = 150$, while in the **right** figure, $N = 2500$ is used. The levels with gray color correspond to states in the half square well potential that move to the continuum region as the number of steps increases.

4. 2D-Square Well Potential

The square 2D potential, although seldom discussed in detail in textbooks, represents a quite interesting problem from the symmetry point of view [9]. The solutions for the confined case with infinite walls are straightforwardly obtained in terms of the direct product of 1D solutions with energies.

$$E_{n_1 n_2} = \frac{\hbar^2 \pi^2}{2\mu L^2}(n_1^2 + n_2^2). \tag{28}$$

This solution presents a degeneracy far from being trivial to be explained. In fact, from the point of view of the geometrical group $\mathcal{C}_{4v}$, the eigenstates present a systematic accidental degeneracy represented by the couple of degenerated levels carrying one-dimensional irreducible representations (irreps), as it is shown in the energy diagram depicted in Figure 10, where energy units were taken to be $\bar{E}_{n_1 n_2} = E_{n_1 n_2}/(\hbar^2 \pi^2 / 2\mu L^2)$. In order to explained this degeneracy, the new symmetry group $\mathcal{G} = \mathcal{T} \wedge \mathcal{C}_{4v}$ was proposed where the accidental degeneracy with respect to the $\mathcal{C}_{4v}$ group renders normal in the new group [9]. This peculiar property is particular to the confined system. When the walls become finite, degeneracy is either partially or completely removed depending of the depth and wide of the well. However, the description of the 2D system for a finite wall is a nontrivial task that will be considered in this work. The aim of this study is to provide physical insight into the symmetry breaking phenomenon induced by the depth of the potential. Starting with a confined particle with symmetry group $\mathcal{G} = \mathcal{T} \wedge \mathcal{C}_{4v}$, which is analyzed in detail in Appendix B, we shall proceed to present the general approach to tackle the 2D system in the framework of algebraic DVR approaches. We strongly recommend reading Appendix B in order to take full advantage of the discussion of this section.

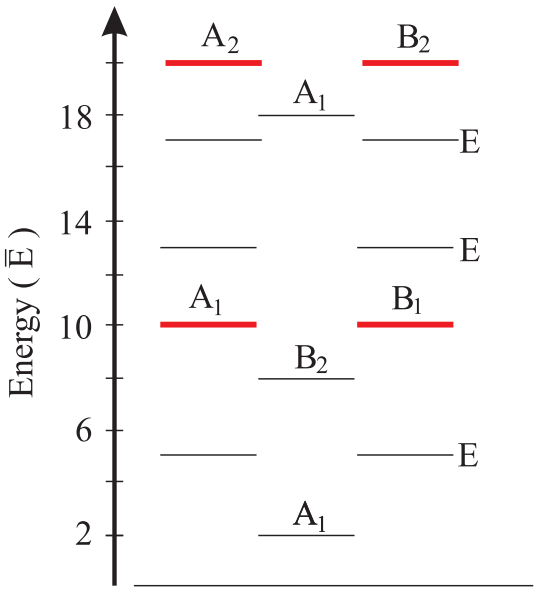

Figure 10. Irreducible representations associated with the energy levels of a particle confined in a square well potential. Systematic accidental degeneracy with irreps (A_1, B_1) and (A_2, B_2) has been remarked. See Leybraz et al. [9].

4.1. Application of the Algebraic DVR Approaches to 2D Systems

Here, we consider a particle in a square well potential with potential depth V_0. This problem will be solved in terms of the direct product of 1D bases corresponding to the x and y axes. In the following discussion, we shall use the HO-DVR method. The procedure using the PT-DVR approach is analogous, and we only have to establish the following mapping: $|n_x\rangle \otimes |n_y\rangle \to |\Phi^{\sigma}_{n_x}\rangle \otimes |\Phi^{\sigma}_{n_y}\rangle$.

The Hamiltonian associated with 2D square potential will be diagonalized in the direct product space of harmonic oscillators given by the following.

$$|n_x n_y\rangle = |n_x\rangle \otimes |n_y\rangle. \tag{29}$$

In order to generate the DVR basis, we first consider the discrete basis associated with the x coordinate, which takes the following form:

$$|x_i\rangle = \sum_{n_x=0}^{N-1} \langle n_x|x_i\rangle |n_x\rangle, \tag{30}$$

$$|p_{xi}\rangle = \sum_{n_x=0}^{N-1} \langle n_x|p_{xi}\rangle |n_x\rangle, \tag{31}$$

with a similar basis for the y degree of freedom.

$$|y_i\rangle = \sum_{n_y=0}^{N-1} \langle n_y|y_i\rangle |n_y\rangle, \tag{32}$$

$$|p_{yi}\rangle = \sum_{n_y=0}^{N-1} \langle n_y|p_{yi}\rangle |n_y\rangle. \tag{33}$$

In terms of discrete bases, the direct product (29) takes the following form.

$$|n_x n_y\rangle = \sum_{i=1}^{N}\sum_{j=1}^{N} \langle x_i|n_x\rangle\langle y_j|n_y\rangle \; |x_i\rangle \otimes |y_j\rangle. \tag{34}$$

It is now convenient to introduce the following notation for the matrix elements involved in the following (34):

$$A_{i,n_x} = \langle x_i|n_x\rangle, \tag{35}$$

$$B_{j,n_y} = \langle y_j|n_y\rangle, \tag{36}$$

$$T_{ij,n_x n_y} = \langle x_i|n_x\rangle\langle y_j|n_y\rangle, \tag{37}$$

with the following relation.

$$\mathbf{T} = \mathbf{A} \otimes \mathbf{B}. \tag{38}$$

In terms of the **T** matrix, the direct product (29) is recast in the following form:

$$|\alpha\rangle = \sum_{\beta=1}^{N^2} T_{\beta,\alpha}|\beta\rangle, \tag{39}$$

where $|\alpha\rangle = |n_x\rangle \otimes |n_y\rangle$ and $|\beta\rangle = |x_i\rangle \otimes |y_j\rangle$, with the following mapping.

$$\alpha = (n_x - 1)N + n_y, \tag{40}$$

$$\beta = (i-1)N + j. \tag{41}$$

Following, the same procedure for the momentum representation, we define the following:

$$C_{i,n_x} = \langle p_{xi}|n_x\rangle, \tag{42}$$

$$D_{j,n_y} = \langle p_{yj}|n_y\rangle, \tag{43}$$

$$W_{ij,n_x n_y} = \langle p_{xi}|n_x\rangle\langle p_{yj}|n_y\rangle, \tag{44}$$

with the direct product basis:

$$|\alpha\rangle = \sum_{\beta=1}^{N^2} W_{\gamma,\alpha}|\gamma\rangle, \tag{45}$$

where $|\alpha\rangle = |n_x\rangle \otimes |n_y\rangle$, $|\gamma\rangle = |p_{xi}\rangle \otimes |p_{yj}\rangle$, and $\gamma = (i-1)N + j$ with the following.

$$\mathbf{W} = \mathbf{C} \otimes \mathbf{D}. \tag{46}$$

Using the direct product bases, the Hamiltonian matrix representation in the framework of the HO-DVR approach takes the following form:

$$\mathbf{H} = \mathbf{W}^{\dagger}\mathbf{\Lambda}^{(\mathbf{p})}\mathbf{W} + \mathbf{T}^{\dagger}\mathbf{\Lambda}^{(V)}\mathbf{T}, \tag{47}$$

where the matrix elements of $\mathbf{\Lambda}^{(\mathbf{p})}$ in the momentum representations are as follows:

$$||\mathbf{\Lambda}^{(\mathbf{p})}|| = \frac{1}{2\mu}(p_{xi}^2 + p_{yj}^2)\delta_{ii'}\delta_{jj'}, \tag{48}$$

while, for the potential in the coordinate representation, we have the following.

$$||\mathbf{\Lambda}^{(V)}|| = V(x_i, y_j)\delta_{ii'}\delta_{jj'}. \tag{49}$$

Hence, the diagonalization of the coordinate and momentum for the 1D systems in x and y provides the discrete localized bases to obtain the Hamiltonian matrix representation in terms of diagonal matrices. The direct product bases possess the relevant property of simplicity; however, the basis dimension increases as N^2, and it may happen that a very large number of direct product functions are necessary for energy convergence. In order to reduce the cost of explicit diagonalization, the Lanczos algorithm may be used, which does not require storage of the Hamiltonian matrix [39]. In addition, it may be possible to reduce the size of the direct product by excluding functions that do not contribute to the associated wave functions involved in the energy levels of interest [41]. Instead, in this contribution, we are simplifying our analysis by introducing symmetry adapted functions. In the framework of this point of view, the projected basis takes the following form:

$$|_q\phi_{\gamma}^{(\Gamma)}\rangle = \sum_{n_x,n_y} S_{n_x n_y;q\Gamma\gamma}|n_x n_y\rangle, \tag{50}$$

where Γ and γ are the irrep and component, respectively, of group $\mathcal{C}_{4v}$. Index q refers to the multiplicity of the irreps and it provides the dimension of the matrix representation to be diagonalized. In this context, the Hamiltonian matrix has the following form:

$$\mathbf{H}_s = \mathbf{S}^{\dagger}[\mathbf{W}^{\dagger}\mathbf{\Lambda}^{(\mathbf{p})}\mathbf{W} + \mathbf{T}^{\dagger}\mathbf{\Lambda}^{(V)}\mathbf{T}]\mathbf{S}, \tag{51}$$

which is in blocked form:

$$\mathbf{H}_s = \sum_{\Gamma} \oplus \mathbf{H}_s^{\Gamma}, \tag{52}$$

where each block is characterized by the one irrep of the group taking the first component for the degenerate irreps. The dimension of each block is given by $q(\Gamma)^2$. We should remark that the use of symmetry, beyond the fact that simplifies the calculation, is a compulsory task because we are interested in identifying the degeneracy associated with symmetry and consequently the levels must carry the corresponding irrep. Symmetry projection, however, is not a trivial task due to the large amount of basis functions involved. Hence, we consider it to be convenient to present a highly efficient symmetry projection approach, which is called the eigenfunction method.

4.2. Symmetry Adapted Basis

In this section, we shall present the application of the eigenfunction method to project the direct product basis (29), which consists in diagonalizing a complete set of commuting operators (CSCO) given in terms of a linear combination of classes [54–57].

The CSCO used to project the basis is defined in accordance with a suitable canonical subgroup chain, which in our case has been chosen to be the following:

$$\mathcal{C}_{4v} \supset \mathcal{C}_s^d, \tag{53}$$

where the following is the case:

$$\mathcal{C}_s^d = \{E, \sigma_d^a\}, \tag{54}$$

with symmetry elements depicted in panel (b) of Figure A1. Denoting the i-th class of group $\mathcal{C}_{4v}$ as K_i and the classes of the subgroup $\mathcal{C}_s^d$ as k_j, we have, for the CSCO called C_{II}, the following linear combination:

$$\hat{C}_{II} = \hat{C}_I^{\mathcal{C}_{4v}} + \hat{C}_I^{\mathcal{C}_s^d}, \tag{55}$$

where the following is the case:

$$\hat{C}_I^{\mathcal{C}_{4v}} = \hat{K}_2 + 3\hat{K}_5; \qquad \hat{C}_I^{\mathcal{C}_s^d} = \hat{k}_2, \tag{56}$$

with the following classes:

$$\hat{K}_2 = \hat{C}_4 + \hat{C}_4^3; \quad \hat{K}_5 = \hat{\sigma}_d^a + \hat{\sigma}_d^b; \quad \hat{k}_2 = \hat{\sigma}_d^a, \tag{57}$$

following the standard class numbering for character tables. Operators $\hat{C}_I^{\mathcal{C}_{4v}}$ and $\hat{C}_I^{\mathcal{C}_s^d}$ distinguish the irreps of groups $\mathcal{C}_{4v}$ and $\mathcal{C}_s^d$, respectively, while operator $\hat{C}_{II}$ distinguishes the irreps and components of group $\mathcal{C}_{4v}$. Their simultaneous diagonalization leads to eigenkets $|\mu\nu\rangle$ defined by the eigensystem:

$$\begin{aligned} \hat{C}_I^{\mathcal{C}_{4v}}|\mu\nu\rangle &= \mu|\mu\nu\rangle; \quad \hat{C}_I^{\mathcal{C}_s^d}|\mu\nu\rangle = \nu|\mu\nu\rangle, \\ \hat{C}_{II}|\mu\nu\rangle &= (\mu+\nu)|\mu\nu\rangle, \end{aligned} \tag{58}$$

where $\mu = \mu(\Gamma)$ and $\nu = \nu(\gamma)$ are functions of the group and the subgroup characters:

$$\mu = \frac{2\chi_2^{(\Gamma)}}{n_\Gamma} + \frac{3\chi_5^{(\Gamma)}}{n_\Gamma}; \qquad \nu = \chi_2^{(\gamma)}, \tag{59}$$

where γ stands for the irrep of subgroup $\mathcal{C}_s^d$, n_Γ refers to the dimension of the Γ-th irrep and $\gamma \in \mathbf{D}^{(\Gamma)}(\mathcal{C}_{4v}) \downarrow \mathcal{C}_s^d$. Hence, the symmetry-adapted functions are equally expressed either with $|\Gamma\gamma\rangle$ or $|\mu\nu\rangle$.

We now have to establish the effect of the operators involved in (55). Since $\hat{C}_4$ and $\hat{\sigma}_d^a$ are generators of the group, it will not be necessary to consider operator $\hat{\sigma}_d^b$. Formally, we start establishing the effect of these operators over the following basis.

$$\begin{aligned} \hat{C}_4|x\rangle &= |C_4 x\rangle = |y\rangle; \qquad \hat{\sigma}_d^a|x\rangle = |\sigma_d^a x\rangle = |y\rangle, \\ \hat{C}_4|y\rangle &= |C_4 y\rangle = |-x\rangle; \quad \hat{\sigma}_d^a|y\rangle = |\sigma_d^a y\rangle = |x\rangle. \end{aligned} \tag{60}$$

Hence, for rotation C_4, we have the following.

$$\begin{aligned}\langle n'_x n'_y|\hat{C}_4|n_x n_y\rangle &= \int_4 dxdydx'dy'\langle n'_x n'_y|x'y'\rangle\langle x'y'|C_4|xy\rangle\langle xy|n_x n_y\rangle \\ &= \int_4 dxdydx'dy'\langle n'_x n'_y|x'y'\rangle\langle xy|n_x n_y\rangle\delta(y-x')\delta(y'+x) \\ &= (-1)^{n_x}\delta_{n'_y n_x}\delta_{n'_x n_y}. \end{aligned} \tag{61}$$

In the similar form, we obtain the following.

$$\langle n'_x n'_y|\hat{C}_4^3|n_x n_y\rangle = (-1)^{n_y}\delta_{n'_y n_x}\delta_{n'_x n_y}, \tag{62}$$

$$\langle n'_x n'_y|\hat{\sigma}_d^a|n_x n_y\rangle = \delta_{n'_y n_x}\delta_{n'_x n_y}, \tag{63}$$

$$\langle n'_x n'_y|\hat{\sigma}_d^b|n_x n_y\rangle = (-1)^{(n_x+n_y)}\delta_{n'_x n_y}\delta_{n'_y n_x}. \tag{64}$$

Gathering all these matrix elements in operator $\hat{C}_{II}$, we obtain the following.

$$\langle n'_x n'_y|\hat{C}_{II}|n_x n_y\rangle = [(-1)^{n_x}+(-1)^{n_y}+4+3(-1)^{n_x+n_y}]\delta_{n'_x n_y}\delta_{n'_y n_x}. \tag{65}$$

Although this matrix representation has dimension N^2, in practice, it is a block diagonal with N one-dimensional matrices and a number of $N(N-1)/2$ two-dimensional matrices for even N, for instance. This fact significantly simplifies the projection. For example, taken $N = 4$ with dimension space $N^2 = 16$, the symmetry projection reduces to the following:

$$\mathcal{L}_{12} = \mathcal{L}_3^{A_1} \oplus \mathcal{L}_1^{A_2} \oplus \mathcal{L}_1^{B_1} \oplus \mathcal{L}_3^{B_2} \oplus \mathcal{L}_4^{E_1}, \tag{66}$$

where of course only the first component of the degenerate irrep E is necessary. Hence, the original Hamiltonian matrix of dimension N^2 given by (47) reduces to the diagonalization of five matrices of dimension a_Γ in accordance to the reduction in representation $\Delta^{(red)}(C_{II})$ given by the following (65).

$$\mathbf{S}^{-1}\Delta^{(red)}(C_{II})\mathbf{S} = \sum_\mu \oplus a_\Gamma \mathbf{D}^\Gamma(C_{II}). \tag{67}$$

We now proceed to take advantage of this projection to obtain the description of the square well potential in the framework of the DVR approach through the diagonalization of the representation matrix (51).

4.3. Results and Discussion

In order to evaluate the validity of our approach, we start considering the case of a square well potential with infinite walls with exact energies given by (28). The parameters were chosen to be $a = 4$ Å and $V_0 = 10^8$ cm^{-1}, with the same mass previously considered. As in the 1D case, we describe the system using both HO-DVR and PT-DVR methods, fitting the parameters ω and α, respectively. The results are displayed in Table 3, where the criterion for the extension of the basis was given by obtaining errors of 1 %. We have carried out calculations with the criterion of choosing the basis dimensions as close as possible but in accordance with an absolute minimum in rms. The basis dimensions are $N = 52$ and $N = 60$ for the HO-DVR and PT-DVR approaches respectively. The results are evaluated at the level of energies and wave functions. Concerning the energy spectrum, both methods present similar errors.

Table 3. Results for one particle confined in a 2D square well potential using both HO-DVR and PT-DVR methods. The fitted parameters were chosen to be $\omega = 2.0 \times 10^{13}$ s^{-1} for the HO-DVR method and $\alpha = 4.5 \times 10^{9}$ m^{-1} for the PT-DVR method. The basis dimensions were chosen to obtain the absolute minimum of rms. Hence, for HO-DVR, we have taken $N = 52$, while for PT-DVR, we have $N = 60$.

			HO-DVR $N^2 = 2704$		**PT-DVR** $N^2 = 3600$	
Irrep	(n_1, n_2)	**Exact (cm^{-1})**	E_c(cm^{-1})	**% Error**	E_c(cm^{-1})	**% Error**
A_1	(1,1)	20.65	20.62	0.14	20.64	0.04
E	(2,1)	51.62	51.57	0.10	51.48	0.27
B_2	(2,2)	82.59	82.49	0.12	82.32	0.33
A_1	(3,1)	103.24	103.25	0.01	103.20	0.04
B_1	(3,1)	103.24	103.25	0.01	103.20	0.04
E	(3,2)	134.22	134.17	0.03	134.04	0.13
E	(4,1)	175.51	175.29	0.13	175.94	0.24
A_1	(3,3)	185.84	186.85	0.54	185.77	0.04
A_2	(4,2)	206.48	206.21	0.13	205.78	0.34
B_2	(4,2)	206.48	206.21	0.13	205.78	0.34

In order to show that the energy convergence showed in Table 3 provides also the correct wave functions, we have projected the eigenvectors to the position representation. Each eigenvector $|\psi_\alpha^{\Gamma\gamma}\rangle$ of Hamiltonian (51) is given in terms of a linear combination of the symmetry adapted basis (50).

$$|\psi_\alpha^{\Gamma,\gamma}\rangle = \sum_q V_{q\alpha}\ |_q\phi_\gamma^{(\Gamma)}\rangle. \tag{68}$$

The wave functions are obtained through the following projection:

$$\psi_\alpha^{\Gamma,\gamma}(x,y) = \langle xy|\psi_\alpha^{\Gamma,\gamma}\rangle = \sum_q V_{q\alpha}\ \langle xy|_q\phi_\gamma^{(\Gamma)}\rangle \tag{69}$$

with the following:

$$\langle xy|_q\phi_\gamma^{(\Gamma)}\rangle = \sum_{n_1,n_2} S_{n_1 n_2;q\Gamma\gamma}\psi_{n_x}(x)\psi_{n_y}(y), \tag{70}$$

where $\psi_{n_x}(x)$ and $\psi_{n_y}(y)$ are 1D harmonic oscillator functions. In Figure 11, a selected set of eigenstates has been depicted. These wave functions are identical to the ones obtained by projecting the exact functions (A52). For the first levels, we have the following correspondence.

$$|\psi_1^{A_1}\rangle \rightarrow |\phi_{11}^{A_1}\rangle; \quad |\psi_1^{B_2}\rangle \rightarrow |\phi_{22}^{B_2}\rangle \tag{71}$$

$$|\psi_2^{A_1}\rangle \rightarrow |\phi_{31}^{A_1}\rangle; \quad |\psi_2^{B_2}\rangle \rightarrow |\phi_{42}^{B_2}\rangle \tag{72}$$

$$|\psi_3^{A_1}\rangle \rightarrow |\phi_{33}^{A_1}\rangle; \quad |\psi_1^{E,A'}\rangle \rightarrow |\phi_{21}^{E,A'}\rangle \tag{73}$$

$$|\psi_1^{A_2}\rangle \rightarrow |\phi_{42}^{A_2}\rangle; \quad |\psi_2^{E,A'}\rangle \rightarrow |\phi_{32}^{E,A'}\rangle \tag{74}$$

$$|\psi_1^{B_1}\rangle \rightarrow |\phi_{31}^{B_1}\rangle; \quad |\psi_3^{E,A'}\rangle \rightarrow |\phi_{41}^{E,A'}\rangle. \tag{75}$$

It should be clear that the labels of these wave functions have their correspondence with the labeling of group $\mathcal{G}$ in accordance with Table A6.

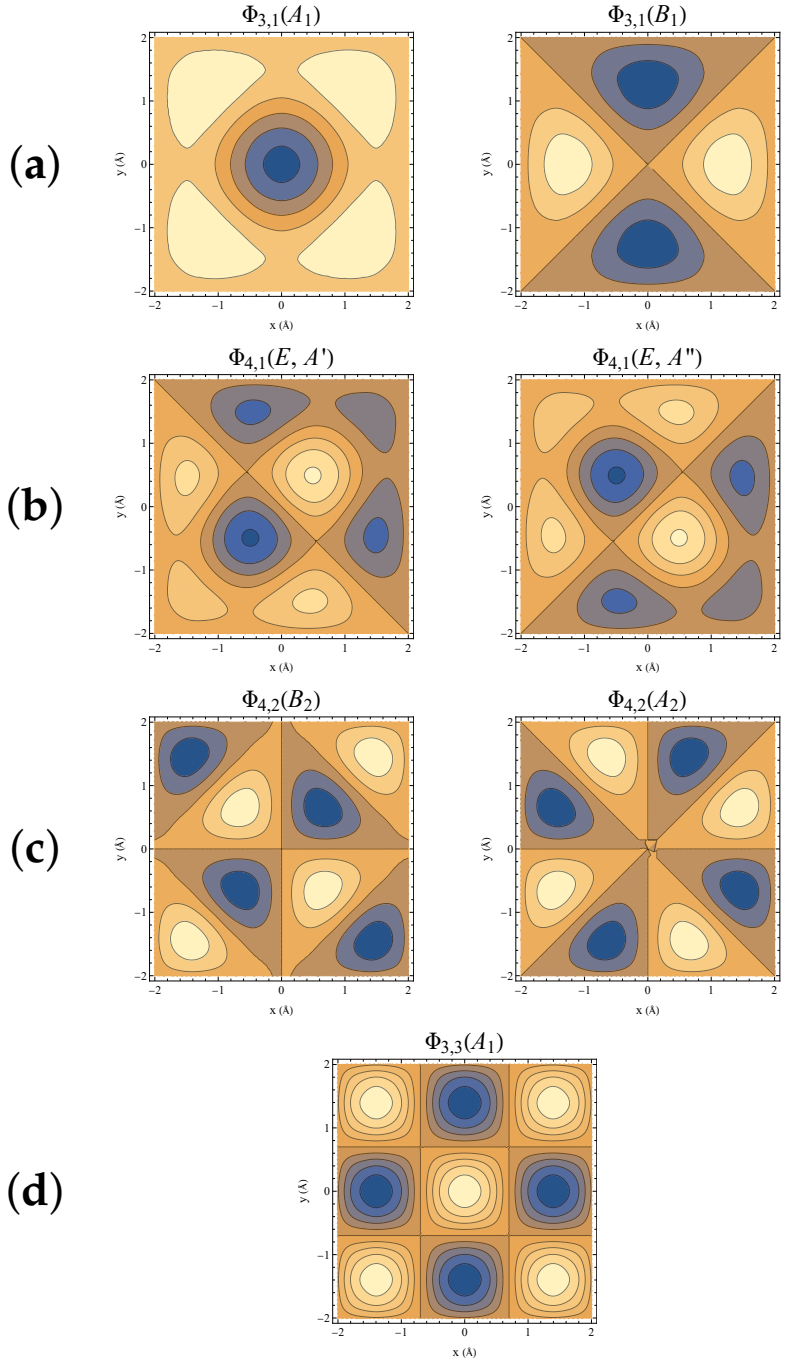

Figure 11. Selected symmetry projected wave functions associated with a particle in a square well potential. Both HO-DVR and PT-DVR provide the same plots at this level of resolution using the parameters associated with Table 3. The pair of wave functions are distributed in accordance with (**a**) accidental degeneracy with irreps (A_1, B_1), (**b**) natural degeneracy with components ($E_{A'}, E_{A''}$), (**c**) accidental degeneracy with irreps (A_2, B_2) and (**d**) totally symmetric single state.

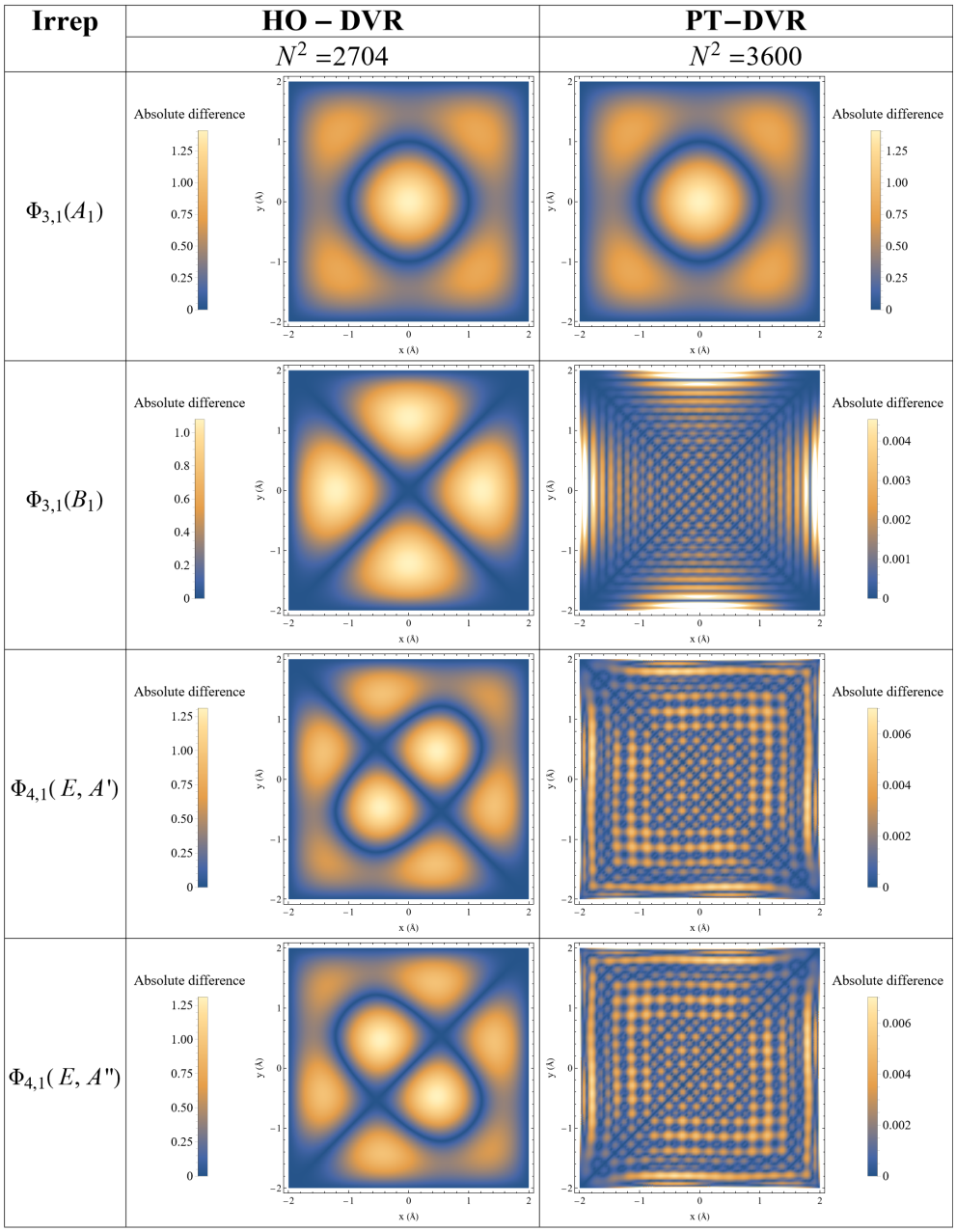

Figure 12. Absolute value of the difference between the exact and calculated wave functions for selected states. The differences show that the PT-DVR approach is more appropriate to describe this system. Hence, for HO-DVR, we have taken $N = 52$, while for PT-DVR, we have $N = 60$.

In Figure 11, we show a set of representative wave functions illustrating the different types of degeneracy. The first row (a) shows the degenerate wave functions (3,1) with irreps (A_1, B_1) and energy $E = 103.24\ \text{cm}^{-1}$. This degeneracy is accidental from the point of view of the $\mathcal{C}_{4v}$ group but natural with respect to the $\mathcal{G}$ group with irrep ${}^{A_1}_{k}\mathcal{G}$. In the second row, (b) we show degenerate wave functions $|\psi_3^{E,A'}\rangle \rightarrow |\phi_{41}^{E,A'}\rangle$, which in both groups render a natural degeneracy, a feature manifested by the fact that they are connected by rotation C_4. In (c), we show the degenerate wave functions $(4, 2)$ corresponding to $|\psi_1^{A_2}\rangle, |\psi_2^{B_2}\rangle$ with energy $E = 206.48\ \text{cm}^{-1}$, which span the two dimensional irrep ${}^{A_2}_{k}\mathcal{G}$, but with accidental degeneracy with respect to the $\mathcal{C}_{4v}$ group. Finally, we show in the last row wave function $|\psi_3^{A_1}\rangle$ with energy $E = 185.84\ \text{cm}^{-1}$, which span the one dimensional irrep ${}^{A_1}_{k_0}\mathcal{G} \downarrow A_1$. On the other hand, the wave functions are compared by plotting the absolute value for the

difference between the exact and calculated wave functions displayed in Figure 12, a result that shows that the PT-DVR approach provides better wave functions.

It is interesting to show the N-dependence of the root mean square deviation, which is displayed in Figure 13. In both methods, the general pattern is similar but the detailed structure is quite different. The PT-DVR approach provides a somewhat more regular pattern. In this approach, potential $V(x_i, y_j)$ is evaluated at the discrete points. From the total number of points N^2, a number of points N_{in} fall inside the box (region with $V_0 = 0$). We may thus define the following:

$$\% \; P = \frac{N_{in}}{N^2} \times 100, \tag{76}$$

as the percentage of points falling inside the box. A significant feature of the N-dependence of convergence is that % P is correlated to rms: a minimum in % P corresponds to minimum in rms. This fact has been pointed out with dashed lines in Figure 13. We should observe, however, that several minima in rms are possible for choosing the basis dimension. We have chosen the criterion to select the first absolute minimum, selecting basis dimensions of the same order for both methods. This is a remarkable feature because it provides us with a criterion to select the appropriate basis dimension N to obtain an improvement. This information can be known before carrying out the calculation, since % P is obtained with the zeros of the polynomials [49]. This fact makes DVR methods efficient.

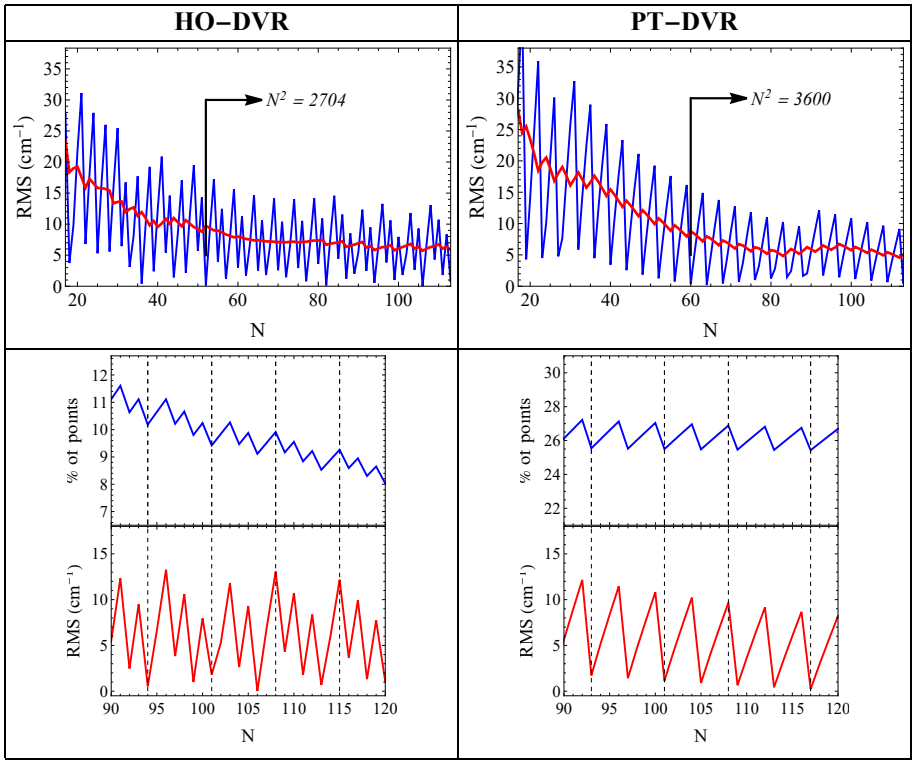

Figure 13. Root mean square deviation as a function of basis dimension N using both HO-DVR and PT-DVR approaches. In the upper panels, the basis dimension N^2 taken to obtain the results of Table 3 is pointed out. The average is included taking into account seven points to the right and to the left when possible. In the lower panels, the corresponding zooms are shown together with the percentage of points % P defined in Equation (76), where its correlation with rms is evident. Notice that several possibilities for the minimum in rms are possible. We have chosen the first absolute minimum in choosing the basis dimension.

The spectrum depicted in Figure 10 is characteristic of the confined particle. When the potential depth becomes finite, the spectrum is expected to be modified in both energy

and degeneracy. The latter feature will be proven by carrying out the calculation with the PT-DVR method.

In Figure 14, we show energy levels as a function of potential depth V_0. It is worth stressing the splitting of the levels (A_1, B_1) and (A_2, B_2) as potential decreases. This means that the true symmetry group becomes geometrical group $\mathcal{C}_{4v}$. In order make the symmetry breaking $\mathcal{G} \downarrow \mathcal{C}_{4v}$ in Figure 15 transparent, a zoom-in of levels (A_1, B_1) and (A_2, B_2) is shown. Notice that levels (A_2, B_2) split sooner than levels (A_1, B_1), which is explained by the fact that states $\{|\phi_{42}^{A_2}\rangle, \phi_{42}^{B_2}\rangle\}$ have higher energies. While the splitting of these levels manifests around $V_0 = 450$ cm^{-1}, the splitting of states $\{|\phi_{31}^{A_1}\rangle, \phi_{31}^{B_1}\rangle\}$ are clearly manifested until $V_0 = 250$ cm^{-1}. This means that, at some values of potential V_0, the systematic accidental degeneracy disappears, but near-degeneracy remains at the low lying region of the spectrum. In order to quantify this statement, we introduce parameter ζ defined as follows [58,59].

$$\zeta = \left| \frac{2}{\pi} \arctan\left(\frac{(E_1 - E_2)}{(E_1 + E_2)/2} \right) \right|. \tag{77}$$

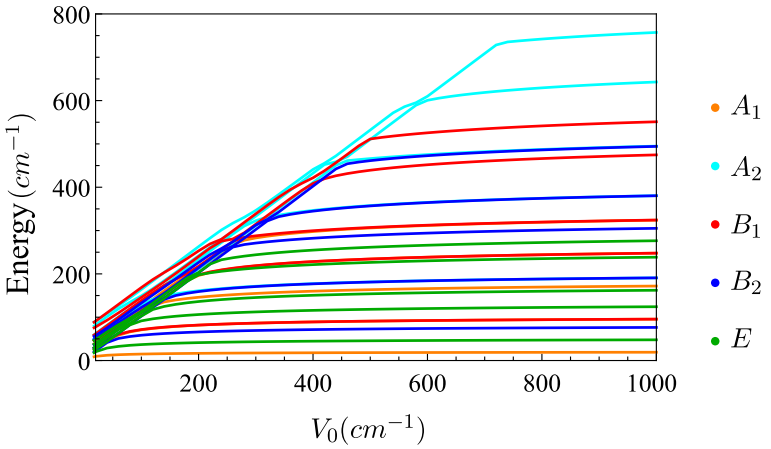

Figure 14. Correlation diagram of energy levels as a function of the potential depth.

This parameter measures the relative splitting between a couple of levels E_1 and E_2. For complete degeneracy $\zeta = 0$, while as splitting increases $\zeta \to 1$. In the same Figure 15, the parameters $\zeta_{A_1B_1}$ and $\zeta_{A_2B_2}$ associated with the degenerate levels for the square well potential are depicted as a function of the potential depth. As the potential depth decreases, the first parameter $\zeta_{A_2B_2}$ starts increasing before $\zeta_{A_1B_1}$. It is until the value of $V_0 = 350$ cm^{-1} that $\zeta_{A_1B_1}$ shows splitting, establishing the limit of accidental degeneracy. Using the PT-DVR approach, we have chosen four potential depths, namely $V_0 = 10^8$, 350, 250 and 180 cm^{-1}, to exemplify the order of splitting induced by the finite potential depth. It is clear that, for potential depth $V_0 = 350$ cm^{-1}, the levels A_1 and A_2 are nearly degenerate, while the splitting of levels A_2 and B_2 becomes manifest. This degeneracy pattern was displayed with a given set of parameters V_0 and wide a, but with the appropriate parameters involving a larger number of bound states and the lower states A_1, B_1 are expected to remain degenerate for finite potential depths. In such situations, an accidental degeneracy remains in the low lying are of the spectrum, with broken degeneracy in the rest of the spectrum. This correlation diagram is has been carried out without taking into account the criterion of % P, and consequently, it cannot be considered as a definitive result. However, it provides proof of symmetry breaking.

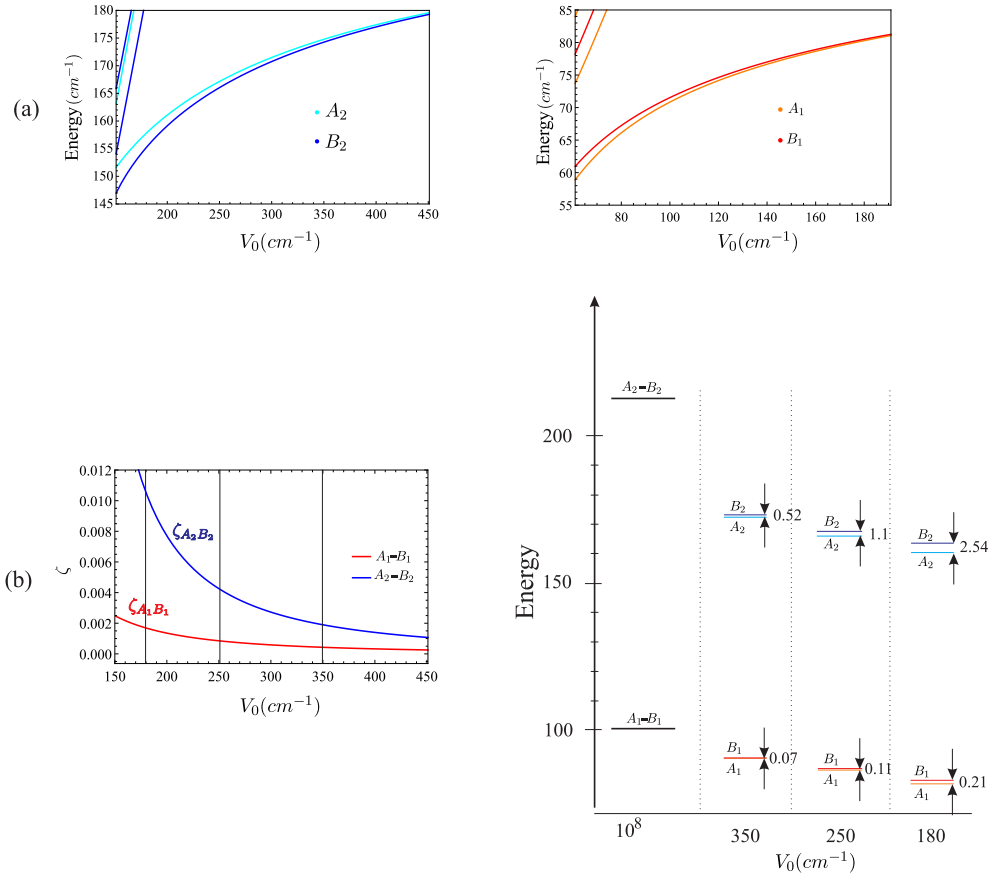

Figure 15. (**a**) A zoom-in of Figure 14 to show the correlation diagram of energy levels $\{A_2, B_2\}$ and $\{A_1, B_1\}$ as a function of the potential. In (**b**), the associated parameters ζ for these couple of levels are shown together with the corresponding energy splitting.

5. 2D-Rectangular Well Potential

In this section, we pay attention to the case of a rectangular square well potential with commensurate sides, as depicted in Figure 16. This case is interesting because systematic accidental degeneracy is also present. As in the square well potential case, the eigenstates —taking the origin in the left bottom corner of the rectangle with sides L_1 and L_2— are given by the following:

$$\Phi_{n_1 n_2}(x, y) = \frac{2}{\sqrt{L_1 L_2}} \sin\left(\frac{n_1 \pi x}{L_1}\right) \sin\left(\frac{n_2 \pi y}{L_2}\right), \tag{78}$$

where n_1 and n_2 are positive integers. The energies levels are given by the following.

$$E_{n_1 n_2} = \frac{\hbar^2 \pi^2}{2\mu}\left(\frac{n_1^2}{L_1^2} + \frac{n_2^2}{L_2^2}\right). \tag{79}$$

The commensurate sides may be imposed by considering the following:

$$nL_1 = mL_2 = L_0, \tag{80}$$

in such a manner that energy takes the following form.

$$E_{n_1 n_2} = \frac{\hbar^2 \pi^2}{2\mu L_0^2}(n^2 n_1^2 + m^2 n_2^2). \tag{81}$$

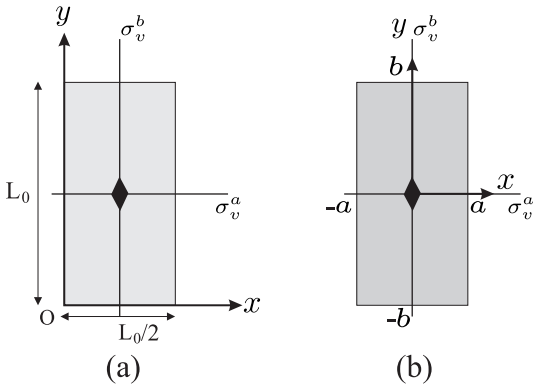

Figure 16. Rectangular well potential and symmetry elements associated with the geometrical symmetry $\mathcal{C}_{4v}$. Two reference systems are shown: (**a**) the origin is located at the left corner with solutions given by (78) and (**b**) the origin is located at the center of the rectangle.

Hence, states $|\psi_{n_1 n_2}\rangle$ and $|\psi_{n_1 n_2}\rangle$ are degenerate if the following is the case.

$$(nn_1)^2 + (mn_2)^2 = (nn_1')^2 + (mn_2')^2. \tag{82}$$

As an example, we shall consider the case where the length in the y direction is twice the length in the x direction, as depicted in Figure 16. In this case, we have $n = 2$ and $m = 1$, which lresults in the following energy expression:

$$\bar{E}_{n_1 n_2} = \frac{E_{n_1 n_2}}{E_0} = (4n_1^2 + n_2^2), \tag{83}$$

where $E_0 = \frac{\hbar^2 \pi^2}{2\mu L_0^2}$. The corresponding spectrum is shown in Figure 17, where the levels with accidental degeneracy have been remarked with broader lines. In this case, the geometrical symmetry is $\mathcal{C}_{2v}$ with eigenfunctions (78) already spanning the irreps shown in Table 4 in accordance with the character in Table 5. The search of a dynamical symmetry leads to operator $\hat{F}^{(A_1)}$, spanning the A_1 irrep:

$$\hat{F}^{(A_1)} = \frac{1}{4}\sqrt{\frac{5}{\pi}}\left(\frac{\partial^2}{\partial x^2} - \frac{\partial^2}{\partial y^2}\right), \tag{84}$$

which connects states B_2. In contrast, it is not possible to find an operator $\hat{D}^{(B_1)}$ from the set of spherical harmonics that preserve the boundary conditions. In Lemus et al. [12], the dynamical operation $\hat{\sigma}_d^a$ was suggested and it connects states A_2 with B_2. Here, we do not intend to obtain irreps based on this idea. Instead, we address the problem of describing accidental degeneracy using DVR approaches and prove that, for finite depth potential, a accidental degeneracy is removed.

To accomplish this task we proceed in similar form to the square well potential. The Hamiltonian associated with the 2D rectangular well potential will be diagonalized in the direct product basis of harmonic oscillators given by the following.

$$|n_x n_y\rangle = |n_x\rangle \otimes |n_y\rangle. \tag{85}$$

In terms of this basis, the Hamiltonian matrix representation takes the following form:

$$\mathbf{H} = \mathbf{W}^\dagger \mathbf{\Lambda}^{(\mathbf{p})} \mathbf{W} + \mathbf{T}^\dagger \mathbf{\Lambda}^{(V)} \mathbf{T}, \tag{86}$$

with the same meaning as in the square well potential. Again, the analysis will be simplified by introducing a symmetry adapted functions through (51), a procedure that should be followed in order to identify accidental degeneracy.

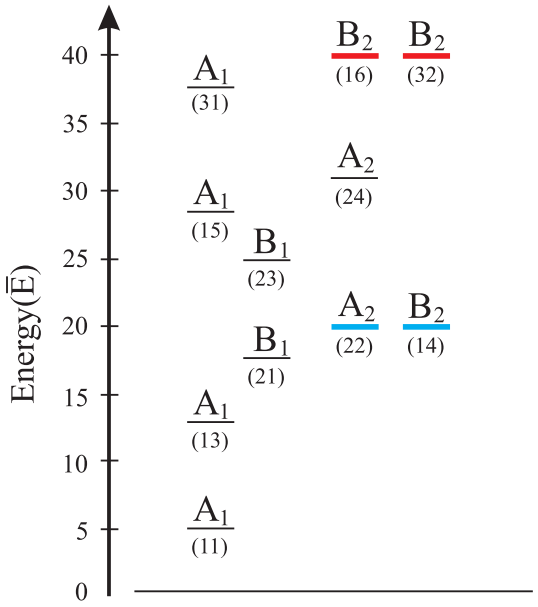

Figure 17. Irreducible representations associated with the energy levels of a particle confined in rectangular wells with $n = 1$ and $m = 2$. Systematic accidental degeneracy with irreps (A_2, B_2) and (B_2, B_2) has been highlighted. The parenthesis $(n_1 n_2)$ corresponds to the labels associated with wave functions (78).

Table 4. Irreps spanned by the functions (78).

Irrep $\mathcal{C}_{2v}$	n_1	n_2
A_1	odd	odd
A_2	even	even
B_1	even	odd
B_2	odd	even

Table 5. Character table for group $\mathcal{C}_{2v}$.

$\mathcal{C}_{2v}$	E	C_2	$\sigma_v(xz)$	$\sigma_v(yz)$		
A_1	1	1	1	1	z	$x^2; y^2; z^2$
A_2	1	1	-1	-1	R_z	xy
B_1	1	-1	1	-1	$x; R_y$	xz
B_2	1	-1	-1	1	$y; R_x$	yz

5.1. Symmetry Adapted Basis

We shall proceed to apply the eigenfunction method to project the direct product basis (29). Since group $\mathcal{C}_{2v}$ presents only one-dimensional irreps, it is enough to consider the following combination of classes.

$$\hat{C} = 3\hat{C}_2 + \hat{\sigma}_v^a. \tag{87}$$

The diagonalization of operators (87) leads to eigenkets $|\mu\rangle$ defined by the eigensystem:

$$\hat{C}|\mu\rangle = \mu|\mu\rangle, \tag{88}$$

where $\mu = \mu(\Gamma)$ is a function of group characters:

$$\mu = 3\chi_2^{(\Gamma)} + \chi_3^{(\Gamma)}, \tag{89}$$

where, here, Γ stands for the irrep of the group $\mathcal{C}_{2v}$. Hence, symmetry-adapted functions are equally expressed either with $|\Gamma\rangle$ or $|\mu\rangle$.

We now have to establish the effect of the operators involved in (87). Formally, we start establishing the effect of these operators over the following basis.

$$\begin{aligned} \hat{C}_2|x\rangle &= |C_2 x\rangle = |-x\rangle; \qquad \hat{\sigma}_v^a|x\rangle = |\sigma_v^a x\rangle = |-x\rangle, \\ \hat{C}_2|y\rangle &= |C_2 y\rangle = |-y\rangle; \qquad \hat{\sigma}_v^a|y\rangle = |\sigma_v^a y\rangle = |y\rangle. \end{aligned} \tag{90}$$

Hence, we have the following.

$$\langle n_x' n_y'|\hat{C}_4|n_x n_y\rangle = (-1)^{n_x+n_y}\delta_{n_x' n_x}\delta_{n_y' n_y}, \tag{91}$$

$$\langle n_x' n_y'|\hat{\sigma}_v^a|n_x, n_y\rangle = (-1)^{n_y}\delta_{n_x' n_x}\delta_{n_y' n_y}. \tag{92}$$

Gathering all these matrix elements in operator $\hat{C}$, we obtain the following.

$$\langle n_x' n_y'|\hat{C}|n_x n_y\rangle = [3(-1)^{n_x+n_y} + (-1)^{n_y}]\delta_{n_x' n_x}\delta_{n_y' n_y}. \tag{93}$$

Notice that this representation matrix is diagonal and, consequently, we use (93) to assign the corresponding irreps to construct the subspaces of symmetry adapted functions.

We now proceed to obtain the description of the rectangular well potential through the diagonalization of the representation matrix (51).

5.2. Results and Discussion

We first consider the case of a rectangular well potential with infinite walls where the exact energies are given by (83). The parameters were chosen to be as follows: $a = 1$ Å , $b = 2$ Å and $V_0 = 10^8$ cm^{-1}. Again, we described the system with both HO-DVR and PT-DVR methods, fitting parameters ω and α, respectively. In this system, because of the different dimensions of the box, two parameters corresponding to the different directions are free to be fitted. The results are displayed in Table 6, where the basis dimension was chosen in accordance with the criterion of % P to obtain a minimum error of 1 %. It is important to remark that the absolute minimum of rms in HO-DVR corresponds to $N = 97$, which is much larger than $N = 73$. For the sake of comparison, we decided to take the values chosen in Table 6 in order to have similar dimensions for both methods.

From these results, we notice that the convergence of the expected degenerate states is difficult to be obtained although, it is quite clear that using the PT-DVR approach results in a better description: with a lower basis dimension, the expected degenerate values are pretty close. In the same venue, in Figure 18, the root mean square deviation is presented, where a similar behavior as in the square well potential is manifested: % P is correlated with the rms. Indeed the best description is obtained for a minimum % P, a fact that allows the search for the best dimension basis before carrying out the calculation.

In order to prove that the energy convergence shown in Table 6 provides the correct wave functions, we proceeded to project the eigenvectors to the position representation. In Figure 19, the functions associated with accidental degeneracy are shown. These functions coincide with the ones obtained by Cartesian solutions (78) and correspond to the following.

$$|\Phi_{14}^{B_2}\rangle \;;\; |\Phi_{22}^{A_2}\rangle, \tag{94}$$

$$|\Phi_{16}^{B_2}\rangle \;;\; |\Phi_{32}^{B_2}\rangle. \tag{95}$$

It is clear that there is no geometrical transformation connecting these functions. The differential operator (84) connects the degenerate B_2 functions but not the states $|\phi_{14}^{B_2}\rangle$ and $|\phi_{22}^{A_2}\rangle$. In Lemus et al. [12], it was suggested that operator $\hat{\sigma}_d^a$ corresponding to the reflection with symmetry element depicted in Figure 20 with the previso that the space must be considered with periodic boundary conditions, which is explained by the need to have well defined functions in the original rectangular box.

Table 6. Results of the energies in cm^{-1} for one particle confined in a rectangular square well potential using both HO-DVR and PT-DVR methods. The dimensions of the rectangular well were chosen to be $a = 1$ Å and $b = 2$ Å with the fitted parameters $\omega_x = 2.0 \times 10^{13}$ s^{-1}, $\omega_y = 4.0 \times 10^{13}$ s^{-1}, and $N = 73$ for the HO-DVR method and $\alpha_x = 9.0 \times 10^9$, $\alpha_x = 4.5 \times 10^9$ m^{-1} and $N = 60$ for the PT-DVR method.

			HO-DVR $N^2 = 5329$		**PT-DVR** $N^2 = 3600$	
Irrep	(n_1, n_2)	**Exact** (cm^{-1})	$E_c(cm^{-1})$	**% Error**	$E_c(cm^{-1})$	**% Error**
A_1	$(1,1)$	51.62	51.18	0.85	51.60	0.04
B_2	$(1,2)$	82.59	82.11	0.58	82.44	0.19
A_1	$(1,3)$	134.22	133.60	0.46	134.16	0.04
B_1	$(2,1)$	175.51	173.99	0.87	174.96	0.31
B_2	$(1,4)$	206.49	205.82	0.32	205.90	0.28
A_2	$(2,2)$	206.49	204.92	0.76	205.80	0.33
B_1	$(2,3)$	258.11	256.40	0.66	257.52	0.23
A_1	$(1,5)$	299.40	298.43	0.32	299.30	0.03
A_2	$(2,4)$	330.38	328.63	0.53	329.25	0.34
A_1	$(3,1)$	382.00	378.19	1.00	381.85	0.04
B_2	$(1,6)$	413.00	409.12	0.94	411.56	0.34
B_2	$(3,2)$	413.00	412.01	0.24	412.69	0.07

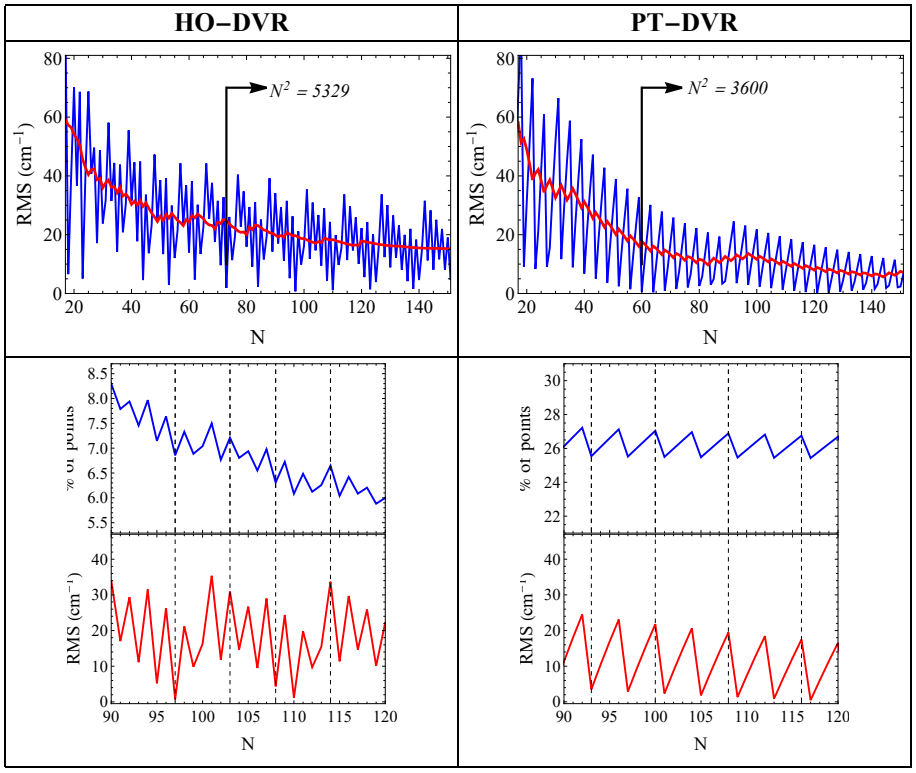

Figure 18. Root mean square deviation as a function of the basis dimension N using both HO-DVR and PT-DVR approaches. In the upper panels, basis dimension N^2 taken to obtain the results of Table 6 are pointed out. The average is included by taking into account seven points to the right and to the left when possible. In the lower panels, the corresponding zooms are shown together with the percentage of points % P defined in Equation (76), where its correlation with rms is evident.

The spectrum of Figure 17 corresponds to a confined particle. When the potential depth becomes finite, the spectrum is modified in both energy and degeneracy. In Figure 21, we show the energy levels as a function of potential depth V_0. As the potential decreases, the

accidental degeneracy associated with levels $\{|\Phi_{16}^{B_2}\rangle, \Phi_{32}^{B_2}\rangle\}$ as well as with $\{|\Phi_{14}^{B_2}\rangle, \Phi_{22}^{A_2}\rangle\}$ is broken. Again, the true symmetry group for the confined particle becomes geometrical group $\mathcal{C}_{2v}$ and no degeneracy appears. The splitting of these couple of levels becomes more evident in the zooms depicted in Figure 22. It is clear that the splitting manifested through function ζ is grater for levels $\{B_2, B_2\}$ than for levels $\{A_2, B_2\}$.

The analysis we have presented for the rectangular well has been limited to ratio $L_1/L_2 = m/n = 1/2$. In order to take into account other possibilities, we shall consider case $m : n = 1/p$ with $p = 1, 2, 3, 4$. In order to achieve this goal, we introduce continuous parameter τ defined as the following.

$$L_2/L_1 = \tau; \;\; \tau : [0.5, 4]. \tag{96}$$

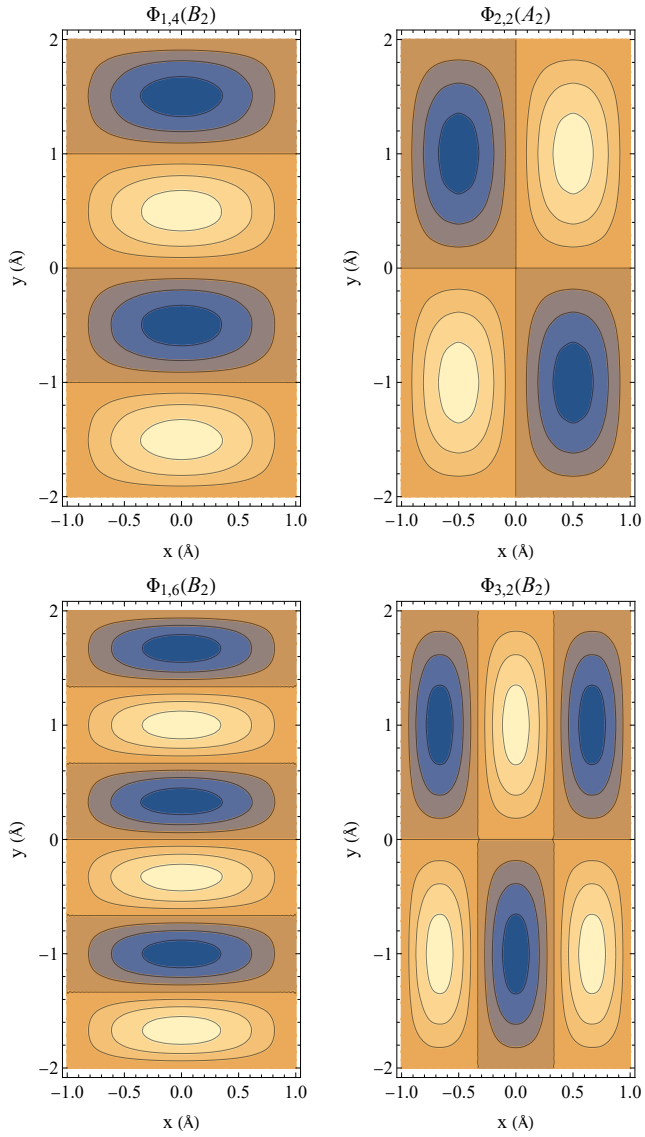

Figure 19. Wave functions associated with a particle in a rectangular well potential calculated with the PT-DVR approach with $N = 60$, in accordance with the results of Table 6. In general, the HO-DVR approach does not provide wave functions of similar quality.

In this manner, we not only consider rectangular boxes with ratios $L_2/L_1 = 2, 3, 4$ but also the case of a square well potential with $\tau = 1$. In Figure 23, we present the energy levels as a function of parameter τ. The diagram was generated using the PT-DVR approach with parameters $N = 60$, $\alpha_x = 9 \times 10^9$ m^{-1} and $\alpha_y = 4.5 \times 10^9$ m^{-1}. The labeling

scheme was chosen in accordance with the $\mathcal{C}_{2v}$ group. For $\tau = 1$, we have the case of a square box. The degenerate states are pointed out with circles and correspond to the pair of levels E and $\{A_2, B_2\}$, which subduce to $B_1 \oplus B_2$ and $\{A_1, A_1\}$, respectively, in $\mathcal{C}_{2v}$. For relation $\tau = 2$, we identify degenerate levels $\{A_2, B_2\}$ and $\{B_2, B_2\}$, which are previously analyzed and provided in Figure 17. For relation $\tau = 3$, two pairs of degenerate levels appear, corresponding to the following levels.

$$|\Phi_{16}^{B_2}\rangle; \qquad |\Phi_{23}^{B_1}\rangle, \tag{97}$$

$$|\Phi_{27}^{B_1}\rangle; \qquad |\Phi_{32}^{B_2}\rangle. \tag{98}$$

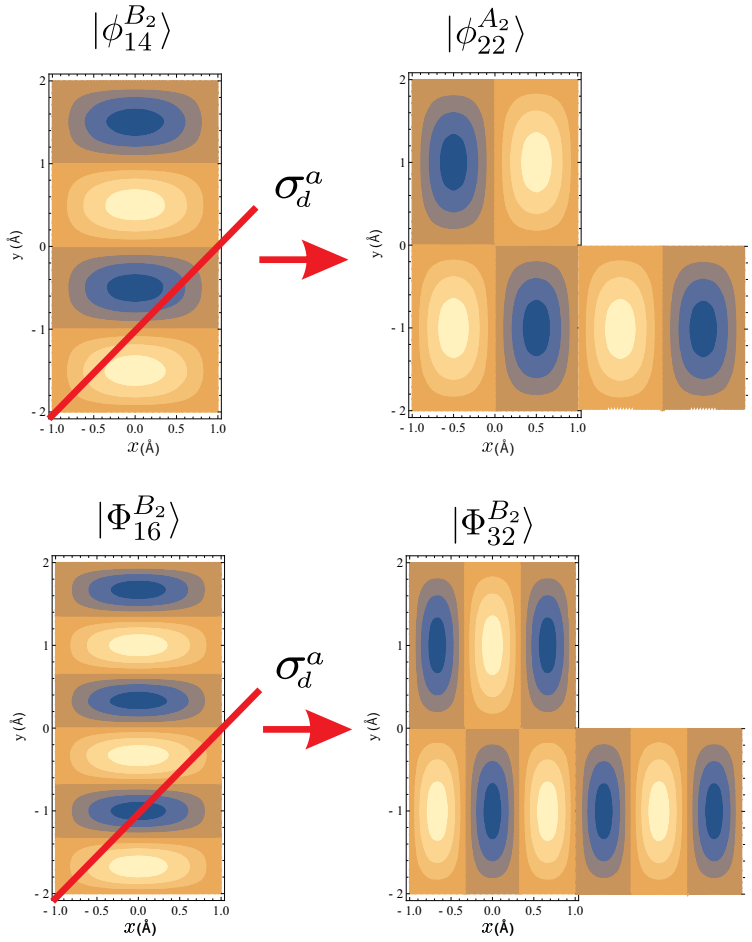

Figure 20. Action of reflection σ_d^a (with symmetry element in red) over the eigenfunctions with accidental degeneracy of the rectangular well potential. At the right of the wave functions the overlap between the original and the resulting wave functions are shown. Although they are coincidental, the space must be extended.

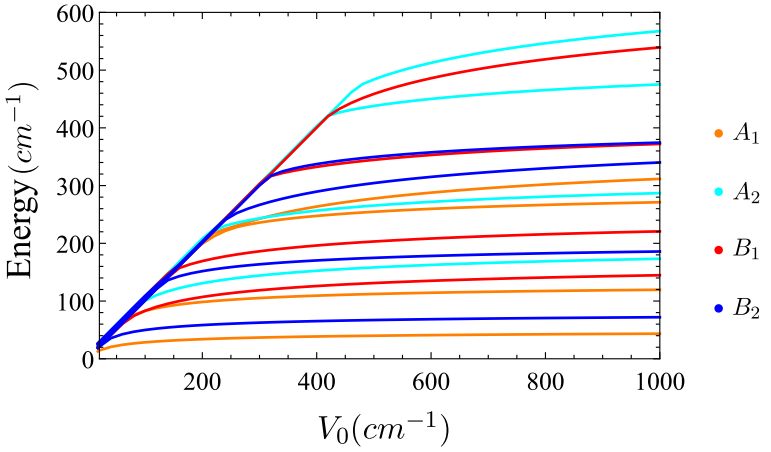

Figure 21. Correlation diagram of the energy levels as a function of the potential depth.

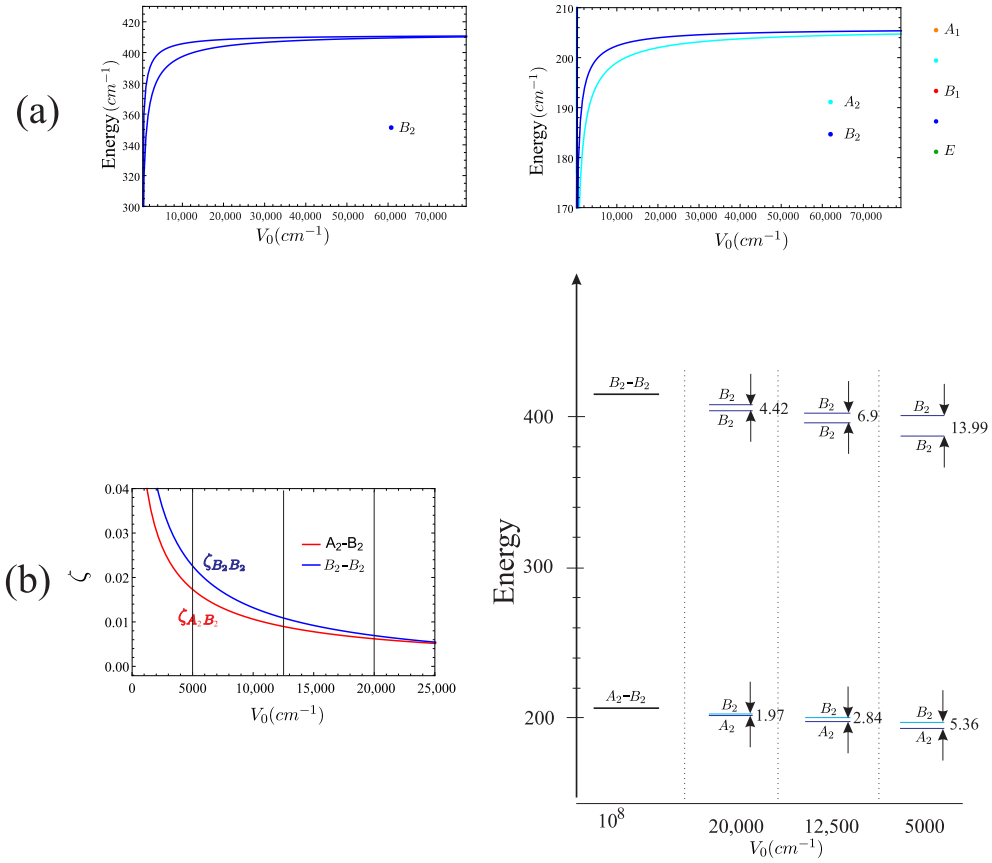

Figure 22. (**a**) A zoom of Figure 21 to show the correlation diagram of the energy levels $\{B_2, B_2\}$ and $\{A_2, B_2\}$ as a function of the potential. In (**b**), the associated parameters ζ for these couple of levels are shown together with the corresponding energy splitting.

Finally, for $\tau = 4$, we have a degeneracy associated to the following states:

$$|\Phi_{17}^{A_1}\rangle; \qquad |\Phi_{21}^{B_1}\rangle, \tag{99}$$

$$|\Phi_{18}^{B_2}\rangle; \qquad |\Phi_{24}^{A_2}\rangle, \tag{100}$$

which are pointed out in the correlation figure. Hence, the diagram of Figure 23 not only allows us to identify the accidental degeneracy due to the commensurate sides, but also shows symmetry breaking when ratio L_2/L_1 stops being an integer. It should be clear that

the accidental degeneracy with respect to group $\mathcal{C}_{2v}$ renders it natural with respect to the true symmetry group.

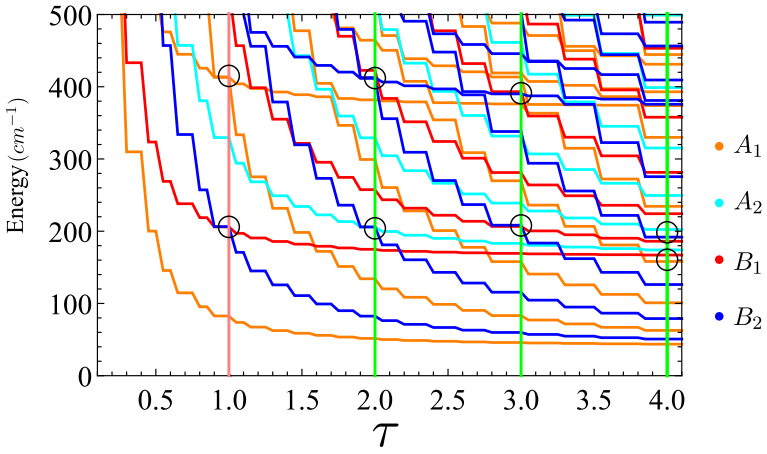

Figure 23. Correlation diagram of the energy levels for a given potential depth as a function of parameter τ defined in (96). The calculation was carried out with the PT-DVR method with parameters $N = 60$, $\alpha_x = 9 \times 10^9$ m^{-1} and $\alpha_y = 4.5 \times 10^9$ m^{-1}. Degeneracy is pointed out with circles. However, for $\tau = 4$, degeneracy is not evident because of lack of convergence.

6. Conclusions

In this contribution, we have presented a quantum mechanical analysis of one particle under 1D and 2D piecewise potentials. First, the benchmark problem of a particle confined in a 1D square well potential was studied in the framework of three methods: HO-DVR, PT-DVR and $SU(2)$-UGA. It was found that the PT-DVR method is the most appropriate approach, albeit the HO-DVR method also provides reasonable results. $SU(2)$-UGA turns out to be inappropriate for these type of potentials. Henceforth, the 1D square well potential with finite walls was studied using these methods. The general trend regarding the advantage of each method remained: A localized discrete basis is the best choice to describe these kind of systems. The next issue we considered was the energy correlation between a spectrum provided by a square and half-space well potentials and the anharmonic spectra associated with realistic interactions such as the case of PT and Morse potentials, respectively. To achieve this task, we have used a multistep piecewise potential. We have shown that the anharmonic spectrum is dominated by the form of the potential near the continuum but not by the presence of the continuum itself. In addition, we confirm the lack of exponential convergence as the basis dimension increases.

As a second issue in our analysis, we have considered a particle confined in a 2D square well potential, a system that is characterized by presenting systematic accidental degeneracy with respect to the geometrical point group $\mathcal{C}_{4v}$. The accidental degeneracy is explained by the identification of a new symmetry group, $\mathcal{T} \wedge \mathcal{C}_{4v}$ [9]. In contrast to the representation analysis provided by Leybraz et al. [9], a formal procedure to construct its irreducible representations is provided. The identification of group $\mathcal{T} \wedge \mathcal{C}_{4v}$ allows us to render systematic accidental degeneracy normal. We have proved that, when the walls of the square well potential become finite, symmetry breaking is present, a phenomenon formally described by the subduction $\mathcal{T} \wedge \mathcal{C}_{4v} \downarrow \mathcal{C}_{4v}$. A relevant aspect of this system with finite walls is that partial symmetry breaking may be manifested depending of the depth of the potential; the low lying levels may still keep accidental degeneracy for a given potential V_0 and width a. Regarding convergence, we have found that the oscillations of the rms displayed in Figure 13 are correlated with the number of discretized points x_i falling inside the square box. Since this number of points corresponds to the zeroes of either the Hermite or Gegenbauer polynomials, the appropriate selection of the basis dimension can be determined before carrying out the calculation. This fact compensates for the lack of exponential convergence. The comparison between the exact results and the calculations obtained by HO-DVR and PT-DVR methods for the confined particle provides

similar results in energy but the PT-DVR approach provides a better description for wave functions.

A square well potential is a quite simple albeit interesting system where all types of degeneracy may be present, a feature that can be used to exemplify the concept of symmetry group and the consequences of not having appropriately identified such group.

It should be stressed that a crucial aspect of this treatment is not only the symmetry projection of the basis to identify degeneracy but also to simplify calculations. The eigenfunction method turns out to be the best option that consists in diagonalizing a complete set of commuting operators defined in terms of a linear combination of classes associated with a chain of groups.

An additional system that we have included in our discussion is the case of a particle confined in a rectangular well potential with commensurate sides. This system also presents systematic accidental degeneracy. We have shown that this degeneracy is removed by the effect of the presence of finite walls. Choosing appropriately the potential depth V_0 and width a, a near-accidental degeneracy may remain for finite walls. We have also shown a correlation of energy levels when, for a given potential depth, the width of the well in the y direction is increased in order to obtain several multiples of the width in the x direction. The depicted correlation plot allows us to identify accidental degeneracy in the form of crossing of levels, a quite enlightening diagram showing the appearance of degeneracy due to commensurability.

Hence, the present analysis shows that algebraic DVR approaches are suitable for dealing with piecewise potentials. In particular, the PT-DVR approach seems to be more appropriate than the HO-DVR method due the fact that the PT-basis carries information of both anharmonicity and the continuum. An analogous situation occurs for the asymmetric square well potential described with the M-DVR approach.

The study we have presented paves the way to explore future applications in the field of quantum chemistry. In particular, the H_2^+ molecule is a good candidate because the evaluation of electron–nuclei interactions is provided as an expansion in terms of spherical harmonics with coefficients depending on the radial coordinate, which behaves as a piecewise potential from the point of view of a DVR approach. A similar situation is present in the Helium atom, although in this case it will be necessary to combine this approach with the transformation brackets introduced by M. Moshinsky [51].

Author Contributions: E.S.: Software, formal analysis, investigation and writing—review and editing; R.D.S.-A.: investigation, validation, writing—review and editing; R.L.: writing—original draft, investigation and supervision. All authors have read and agreed to the published version of the manuscript.

Funding: This work is partially supported by DGAPA-UNAM, Mexico, under project IN-212020.

Institutional Review Board Statement: Not applicable.

Informed Consent Statement: Not applicable.

Data Availability Statement: Not applicable.

Conflicts of Interest: The authors declare no conflict of interest.

Appendix A. Alternative DVR Methods

In this appendix, we present the main features of the algebraic Pöschl-Teller-DVR (PT-DVR), Morse-DVR (M-DVR) and the $SU(2)$-UGA approaches. With the exception of M-DVR approach, these methods are appropriate for symmetric potentials. We start with the PT-DVR approach.

Appendix A.1. PT-DVR Method

The bound states of the Pöschl-Teller potential do not form a complete set of states in the Hilbert space [60–62]. The DVR approach needs a complete basis, which is provided by the following [63]:

$$\Phi_n^\sigma(u) = A_n^\sigma (1-u^2)^{\frac{\sigma}{2}} C_n^{\sigma-1/2}(u); \qquad n = 0, 1, 2, \ldots, \tag{A1}$$

where $C_n^{\sigma-1/2}(u)$ are the Gegenbauer polynomials [64] with argument $u = \tanh(\alpha q)$, and σ is taken to be $\sigma = 1$ in order to decouple the bound from the continuum spectrum [63], while the normalization constant is as follows.

$$A_n^\sigma = \sqrt{\frac{\alpha n!(\sigma+n-1/2)(\Gamma[\sigma-1/2])^2}{\pi 2^{2-2\sigma}\Gamma[2\sigma+n-1]}}. \tag{A2}$$

Using the factorization method, it is possible to obtain ladder operators $\{\hat{K}_\pm, \hat{K}_0\}$ with the following effect [63]:

$$\hat{K}_+\Phi_n^\sigma(u) = k_+\Phi_{n+1}^\sigma(u), \tag{A3}$$
$$\hat{K}_-\Phi_n^\sigma(u) = k_-\Phi_{n-1}^\sigma(u), \tag{A4}$$
$$\hat{K}_0\Phi_n^\sigma(u) = k_0\Phi_n^\sigma(u), \tag{A5}$$

with the following being the case.

$$k_+ = \sqrt{(n+1)(2\sigma+n-1)}, \tag{A6}$$
$$k_- = \sqrt{n(2\sigma+n-2)}, \tag{A7}$$
$$k_0 = (n+\sigma-1/2). \tag{A8}$$

Based on these results, the momentum and natural variable u take the following form [63]:

$$\hat{p} = \frac{i\hbar\alpha}{2}[\hat{B}_+ - \hat{B}_-]; \qquad \hat{u} = \frac{1}{2}[\hat{A}_+ + \hat{A}_-]; \tag{A9}$$

where the new operators are defined by the following actions over the basis.

$$\hat{A}_+\Phi_n^\sigma(u) = \sqrt{\frac{(n+1)(2\sigma+n-1)}{(n+\sigma-1/2)(n+\sigma+1/2)}}\Phi_{n+1}^\sigma(u), \tag{A10}$$
$$\hat{A}_-\Phi_n^\sigma(u) = \sqrt{\frac{n(2\sigma+n-2)}{(n+\sigma-1/2)(n+\sigma-3/2)}}\Phi_{n-1}^\sigma(u), \tag{A11}$$
$$\hat{B}_+\Phi_n^\sigma(u) = (\sigma+n)\hat{A}_+\Phi_n^\sigma(u), \tag{A12}$$
$$\hat{B}_-\Phi_n^\sigma(u) = (\sigma+n-1)\hat{A}_-\Phi_n^\sigma(u). \tag{A13}$$

Using these expressions, we can obtain the matrix elements of the coordinate and momentum, which induces diagonalization in the following subspace:

$$\mathcal{L}_N^{\text{CPT}} = \{|\Phi_n^\sigma\rangle, n = 0, 1, \ldots, N-1\}, \tag{A14}$$

and it induces the following eigenvectors:

$$|u_i\rangle = \sum_{n=0}^{N-1}\langle\Phi_n^\sigma|u_i\rangle|\Phi_n^\sigma\rangle, \tag{A15}$$
$$|p_i\rangle = \sum_{n=0}^{N-1}\langle\Phi_n^\sigma|p_i\rangle|\Phi_n^\sigma\rangle, \tag{A16}$$

which provide momentum and coordinate representations characterized by the following.

$$u|u_i\rangle = u_i|u_i\rangle, \qquad p|p_i\rangle = p_i|p_i\rangle. \tag{A17}$$

For the coordinate, we have relation $u = \tanh(\alpha q)$ and, consequently, the following:

$$\langle u_j|V(q)|u_i\rangle = V[q_i(u_i)]\delta_{ij}, \qquad \langle p_j|G(p)|p_i\rangle = G(p_i)\delta_{ij}, \tag{A18}$$

with the following being the case.

$$q_i = \frac{1}{\alpha}\text{arctanh}(u_i). \tag{A19}$$

Accordingly, the matrix representation of a Hamiltonian associated with a general potential takes the same form (13), albeit with new definitions $\mathbf{T} = ||\langle\Phi_n^\sigma|u_i\rangle||$ and $\mathbf{W} = ||\langle\Phi_n^\sigma|p_i\rangle||$, with $||\mathbf{\Lambda}^{(p)}|| = (p_i^2/2\mu)\delta_{ij}$ and $||\mathbf{\Lambda}^{(q)}|| = V[q_i(u_i)]\delta_{ij}$ in the momentum and coordinate representations, respectively.

Appendix A.2. SU(2)-UGA-DVR Method

The 1D unitary group approach has already been established by Lemus [43,44]. Here, we present salient features of the method. In this approach, a scalar boson $s^\dagger(s)$ is added to the physical space of a 1D harmonic oscillator with bosonic operators $t^\dagger(t)$, called $a^\dagger(a)$ in Section 2. The bilinear products satisfy commutations relations associated with the generators of the $U(2)$ group with the constraint that $\hat{N} = t^\dagger t + s^\dagger s \equiv \hat{n} + \hat{n}_s$ is preserved. A convenient form to express its generators is the following:

$$G_{U(2)} = \{\hat{N}, \hat{J}_x, \hat{J}_y, \hat{J}_z\}, \tag{A20}$$

with the following being the case.

$$\hat{J}_x = \frac{1}{2}(t^\dagger s + s^\dagger t); \qquad \hat{J}_y = -\frac{i}{2}(t^\dagger s - s^\dagger t); \qquad \hat{J}_z = \frac{1}{2}(t^\dagger t - s^\dagger s). \tag{A21}$$

From this perspective, any dynamical variable of a 1D system may be expanded in terms of the generators (A20). The $SU(2)$ group presents three group chains:

$$SU(2) \supset U(1), \tag{A22}$$
$$SU(2) \supset SO(2), \tag{A23}$$
$$SU(2) \supset S\bar{O}(2), \tag{A24}$$

and each of them is characterized by operators $\hat{J}_z$, $\hat{J}_x$ and $\hat{J}_y$, respectively, with the following eigenkets:

$$\hat{J}_z|[N]\mu\rangle = \mu|[N]\mu\rangle = \mu|[N]n\rangle, \tag{A25}$$
$$\hat{J}_x|[N]\zeta\rangle = \zeta|[N]\zeta\rangle, \tag{A26}$$
$$\hat{J}_y|[N]\bar{\zeta}\rangle = \bar{\zeta}|[N]\bar{\zeta}\rangle, \tag{A27}$$

and the following eigenvalues:

$$\mu, \zeta, \bar{\zeta} = -\frac{N}{2}, -\frac{N}{2}+1, \ldots \frac{N}{2}, \tag{A28}$$

with the following relation between μ and the physical quantum number n:

$$n = j + \mu; \qquad N - n = j - \mu, \tag{A29}$$

and j standing for the *angular momentum* associated with the $SU(2)$ group. Since coordinate q and momentum p have the following realization:

$$q \to \hat{\mathcal{Q}} = \frac{1}{\sqrt{2}}\sqrt{\frac{\hbar}{\omega\mu}}\frac{2\hat{J}_x}{\sqrt{N}}, \qquad p \to \hat{\mathcal{P}} = -\frac{1}{\sqrt{2}}\sqrt{\hbar\omega\mu}\frac{2\hat{J}_y}{\sqrt{N}}, \tag{A30}$$

the bases (A26) and (A27) correspond to coordinate and momentum representations, respectively. We stress that the spectra of the coordinate and momentum are discrete, establishing a DVR approach.

The algebraic representation of any 1D system of the following:

$$\hat{H}^{SU(2)}_{alg} = \frac{1}{2\mu}\hat{\mathcal{P}}^2 + V(\hat{\mathcal{Q}}) \tag{A31}$$

is obtained through mapping $q \to \hat{\mathcal{Q}}; p \to \hat{\mathcal{P}}$. Here, it is necessary to add and subtract a quadratic term in such a manner that the harmonic oscillator Hamiltonian is identified. We thus obtain the following:

$$H^{SU(2)}_{\text{alg}} = \hbar\omega\left(\hat{n} + \frac{1}{2} - \frac{\hat{n}^2}{N}\right) + V'(\hat{\mathcal{Q}}), \tag{A32}$$

where the following is the case.

$$V'(\hat{\mathcal{Q}}) = -\frac{\omega^2\mu}{2}\hat{\mathcal{Q}}^2 + V(\hat{\mathcal{Q}}). \tag{A33}$$

Using transformation brackets of the following:

$$\mathbf{T} = ||\langle[N]\zeta|[N]n\rangle||, \tag{A34}$$

associated with the coordinates, the Hamiltonian in the energy representation takes the following form [43,44].

$$\mathbf{H} = \mathbf{\Lambda}^{(E)} + \mathbf{T}^{\dagger}\mathbf{\Lambda}^{(\mathcal{Q})}\mathbf{T}. \tag{A35}$$

A remarkable fact of this approach is that the kets $|[N]n\rangle$ are identified with the 1D harmonic oscillator, and consequently, it is possible to project kets $|[N]\zeta\rangle$ and $|[N]\tilde{\zeta}\rangle$ to position representations. It is important to take into account that, in the UGA, an accidental degeneracy appears, which must be removed [43,44]. This goal is achieved by introducing parameter ϵ in the matrix representation of the deformed oscillator contribution:

$$||\mathbf{\Lambda}^{(E)}|| = \left[\hbar\omega\left(n + \frac{1}{2} - \epsilon\frac{n^2}{N}\right)\right]\delta_{n',n}, \tag{A36}$$

where $\epsilon = 1$ for $n < N/2$ and $\epsilon = 0$ for $n \geq N/2$.

Appendix A.3. Morse DVR Method (M-DVR)

As in the case of the PT potential, the bound states of the Morse potential do not form a complete set of states in the Hilbert space [65,66]. The DVR approach needs a complete basis, which is provided by the tridiagonal Morse basis (TMB) given by the following [67–70]:

$$\Phi^{\sigma}_n(y) = A^{\sigma}_n L^{2\sigma-1}_n(y)\, y^{\sigma} e^{-y/2}, \tag{A37}$$

with the following normalization constant: $A^{\sigma}_n = \sqrt{(\beta n!)/\Gamma(2\sigma+1)}$, where σ is a parameter that is chosen to be $\sigma = 1$ since, in this case, the bound states and the continuum

part of the spectrum are decoupled [69]. Natural variable y is connected with the physical coordinate q through the following:

$$y = (2j+1)e^{-\beta q}, \tag{A38}$$

where j is related to the potential depth and β stands for the range of the Morse potential.

It is possible to construct ladder operators $\{\hat{K}_\pm, \hat{K}_0\}$ satisfying the $su(1,1)$ commutation relations with the following effect over the following basis (A37).

$$\hat{K}_-\Phi_n^\sigma(y) = k_-(n)\,\Phi_{n-1}^\sigma(y) \qquad \text{with} \qquad k_-(n) = \sqrt{n(2\sigma+n-1)}, \tag{A39}$$

$$\hat{K}_+\Phi_n^\sigma(y) = k_+(n)\,\Phi_{n+1}^\sigma(y) \qquad \text{with} \qquad k_+(n) = \sqrt{(n+1)(2\sigma+n)}, \tag{A40}$$

$$\hat{K}_0\Phi_n^\sigma(y) = k_0\Phi_n^\sigma(y) \qquad \text{with} \qquad k_0 = \sigma + n. \tag{A41}$$

On the other hand, natural variable y and momentum $p = -i\hbar\frac{d}{dq}$ are related to the operators (A39)–(A41) in the following form:

$$p = \frac{i\hbar\beta}{2}(\hat{K}_+ - \hat{K}_-), \tag{A42}$$

$$y = 2\hat{K}_0 - (\hat{K}_+ + \hat{K}_-), \tag{A43}$$

with the following matrix elements.

$$\langle\Phi_{n'}^\sigma|y|\Phi_n^\sigma\rangle = 2(\sigma+n)\delta_{n,n'} - (k_+(n)\,\delta_{n',n+1} + k_-(n)\,\delta_{n',n-1}), \tag{A44}$$

$$\langle\Phi_{n'}^\sigma|p|\Phi_n^\sigma\rangle = \frac{i\hbar\beta}{2}(k_+(n)\,\delta_{n',n+1} - k_-(n)\,\delta_{n',n-1}). \tag{A45}$$

The diagonalization of these matrix representations in the following subspace:

$$\mathcal{L}_N^{\text{TMB}} = \{|\Phi_n^\sigma\rangle, n = 0, 1, \ldots, N-1\}, \tag{A46}$$

produces the following eigenvectors:

$$|y_i\rangle = \sum_{n=0}^{N-1}\langle\Phi_n^\sigma|y_i\rangle|\Phi_n^\sigma\rangle, \tag{A47}$$

$$|p_i\rangle = \sum_{n=0}^{N-1}\langle\Phi_n^\sigma|p_i\rangle|\Phi_n^\sigma\rangle, \tag{A48}$$

where matrices $\mathbf{T} = ||\langle\Phi_n^\sigma|y_i\rangle||$ and $\mathbf{W} = ||\langle\Phi_n^\sigma|p_i\rangle||$ correspond to the coefficients that define basis transformations (A47) and (A48), which provide the coordinate and momentum representations characterized by the following.

$$y|y_i\rangle = y_i|y_i\rangle, \qquad p|p_i\rangle = p_i|p_i\rangle. \tag{A49}$$

For the coordinate, we have relation (A38) and, consequently, the following:

$$\langle y_j|V(q)|y_i\rangle = V[q_i(y_i)]\delta_{ij}, \qquad \langle p_j|G(p)|p_i\rangle = G(p_i)\delta_{ij}, \tag{A50}$$

with the following being the case.

$$q_i = -\frac{1}{\beta}\ln\frac{y_i}{(2j+1)}. \tag{A51}$$

Equations (A50) establish the discrete variable representation and relation (A51) allows the description of systems beyond the Morse potential. Following the same procedure,

the matrix representation of a Hamiltonian takes the same form (13) with the appropriate identification of the transformation coefficients and connection (A51).

Appendix B. Symmetry Group and Irreducible Representations

In this section, we present the symmetry group of particle in a 2D square potential with infinite walls together with the construction of its irreducible representations. Although this problem has already been presented in heuristic manner [9], it has not been formally presented in the framework of induced representations as it was for the cubic 3D square well potential [11].

Let us first start by presenting the solutions of one particle inside the potential depicted in Figure A1, where the origin is located at the left corner of the square. In this reference framework, the solutions take the following simple form:

$$\psi_{n_1 n_2}(x,y) = \psi_{n_1}(x)\psi_{n_2}(y), \tag{A52}$$

where the following is the case.

$$\psi_{n_1}(x) = \sqrt{\frac{2}{L}}\sin\left(\frac{n_1\pi x}{L}\right), \tag{A53}$$

$$\psi_{n_2}(y) = \sqrt{\frac{2}{L}}\sin\left(\frac{n_2\pi y}{L}\right). \tag{A54}$$

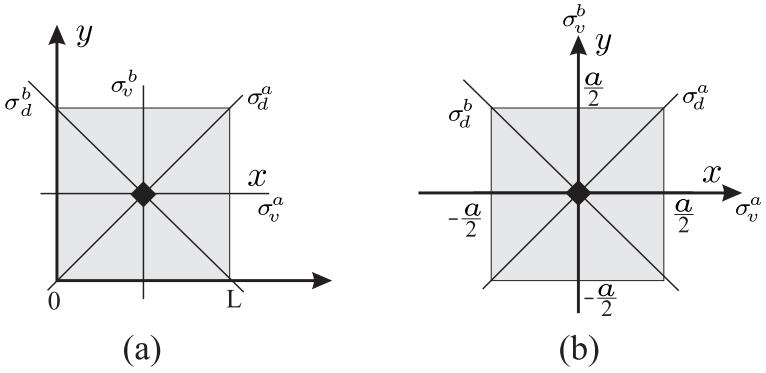

Figure A1. Square well potential and symmetry elements associated with geometrical symmetry $\mathcal{C}_{4v}$. Two reference systems are shown: (**a**) the origin is located at the left corner with solutions given by (A53) and (A54); and (**b**) the origin is located at the center of the square.

The symmetry projection of functions (A52) allows the assignment of irreducible representation to the energy spectrum depicted in Figure 10 [9]. In this system, we are able to identify two subspaces. The one-dimensional space of the following:

$$\mathcal{L}_1 = \{|\psi_{nn}\rangle\} \tag{A55}$$

with the following reduction:

$$|\psi_{nn}^{B_2,A'}\rangle = \quad n \text{ even} \tag{A56}$$

$$|\psi_{nn}^{A_1,A'}\rangle = \quad n \text{ odd}, \tag{A57}$$

and the following two dimensional subspaces:

$$\mathcal{L}_2 = \{|\psi_{nm}\rangle\}; \quad n \neq m, \tag{A58}$$

with reductions provided in Table A1 is provided. The first 13 energy levels obtained with Equation (28) in dimensionless units $\bar{E} = E/(\hbar^2\pi^2/2mL^2)$ are displayed in Figure 10. It is, thus, clear that double degeneracy $A_1 \oplus B_1$ and $A_2 \oplus B_2$ represent accidental degeneracy.

Table A1. Irreducible representations (irreps) of the geometrical group $\mathcal{C}_{4v}$ contained in the subspaces (A58). The reduction depends of the parity of n and m with p and q integers.

Irrep	n	m
E	$2p$	$2q+1$
E	$2p+1$	$2q$
$A_1 \oplus B_1$	$2p+1$	$2q+1$
$A_2 \oplus B_2$	$2p$	$2q$

However, since this degeneracy is systematic over the entire spectrum, we have the presence of systematic accidental degeneracy, which implies that symmetry group $\mathcal{C}_{4v}$ is a subgroup of the true symmetry group. In order to obtain the true symmetry group, it is necessary to identify the operator connecting the accidental degenerate states. In order to achieve this goal, we start establishing that such operators $\hat{F}^{(\rho)}$, carrying the ρ-th irreducible representation (irrep), must satisfy the following.

$$\langle \psi^{\Gamma} | \hat{F}^{(\rho)} | \psi^{\Gamma'} \rangle \neq 0; \quad \text{for} \quad (\Gamma = A_1, \Gamma' = B_1) \text{ and } (\Gamma = A_2, \Gamma' = B_2). \tag{A59}$$

In other words, the operator must span the irrep ρ satisfying the following.

$$\Gamma \in \rho \otimes \Gamma'. \tag{A60}$$

In accordance with the character in Table A2, such operators should span the irreducible representation $\rho = B_1$. Notice that degenerate states $|\psi_i^E\rangle$ are left unaltered by the B_1 tensor.

Table A2. Character table of group $\mathcal{C}_{4v}$.

$\mathcal{C}_{4v}$	E	$2C_4$	C_2	$2\sigma_v$	$2\sigma_d$		
A_1	1	1	1	1	1	z	$x^2+y^2; z^2$
A_2	1	1	1	-1	-1	R_z	
B_1	1	-1	1	1	-1		x^2-y^2
B_2	1	-1	1	-1	1		xy
E	2	0	-2	0	0	$(x,y); (R_x, R_y)$	(xz, yz)

From the character in Table A2, we see that the Cartesian harmonic $x'^2 - y'^2$ spans irrep B_1, where the primes mean that the function is referred to the origin located in panel (b) of Figure A1. However, the same linear combination in terms of the square momenta transforms according to B_1 and, consequently, we have the following operator.

$$\hat{F}^{(B_1)} = \frac{1}{4}\sqrt{\frac{5}{\pi}}\left(\frac{\partial^2}{\partial x^2} - \frac{\partial^2}{\partial y^2}\right). \tag{A61}$$

This operator commutes with the following Hamiltonian:

$$[\hat{H}, \hat{F}^{(B_1)}] = 0, \tag{A62}$$

and conserves boundary conditions. Consequently, it is suitable to be added to the symmetry elements of the $\mathcal{C}_{4v}$ group. Operator (A61) generates continuous group $\mathcal{T}$ with elements obtained by exponentiation in the following manner.

$$\hat{U}(\alpha) = e^{i\alpha \hat{F}^{(B_1)}}. \tag{A63}$$

In order to elucidate the structure of the new group it is convenient to observe whether subgroup $\mathcal{T}$ is invariant. Taking into account that elements $R \in \mathcal{C}_{4v}$ are isomorphic to operators $\hat{\mathcal{O}}_R$ that act over the space of functions, the conjugation of $\hat{U}(\alpha)$ with respect to the elements of $\mathcal{C}_{4v}$ yields the following:

$$\hat{\mathcal{O}}_R \hat{U}(\alpha) \hat{\mathcal{O}}_R^{-1} = \hat{U}(\alpha') \in \mathcal{T}, \tag{A64}$$

with the following being the case:

$$\alpha' = \alpha \chi^{B_1}(R), \tag{A65}$$

where $\chi^{B_1}(R)$ denotes the character of the irrep B_1 in group $\mathcal{C}_{4v}$. This result means that group $\mathcal{T}$ is invariant, a fact that allows the new symmetry group $\mathcal{G}$ to be expressed as a semidirect product:

$$\mathcal{G} = \mathcal{T} \wedge \mathcal{C}_{4v}, \tag{A66}$$

and in terms of an expansion of left cosets.

$$\mathcal{G} = \sum_{\lambda=1}^{|\lambda|} s_\lambda \, \mathcal{T}; \quad |\lambda| = \frac{|\mathcal{G}|}{|\mathcal{T}|}; \quad s_\lambda \in \mathcal{C}_{4v}. \tag{A67}$$

Hence, any element $g \in \mathcal{G}$ can be written in the following form:

$$\hat{g} = \hat{\mathcal{O}}_R \hat{U}(\alpha); \quad R \in \mathcal{C}_{4v}, \tag{A68}$$

where we have simplified the following notation $\hat{g} = \hat{\mathcal{O}}_g$.

We now proceed to construct irreducible representations of group $\mathcal{G}$. To accomplish this task, we shall proceed through the induction method by constructing the irreps of group $\mathcal{G}$ from the irreps of subgroup $\mathcal{T}$. We start with the construction of the irreps of the invariant subgroup, $\mathcal{T}$.

First, let us consider the two dimensional representation spaces.

$$\mathcal{L}_2 = \{|\psi_{n_1 n_2}\rangle, |\psi_{n_2 n_1}\rangle\}; \qquad n_1 \neq n_2. \tag{A69}$$

The action of the elements of $\mathcal{T}$ over this space is given by the following:

$$\hat{U}(\alpha)|\psi_{n_1 n_2}\rangle = D^{(k_{\mathbf{n}})}(\alpha)|\psi_{n_1 n_2}\rangle \tag{A70}$$

where the following is the case:

$$D^{(k_{\mathbf{n}})}(\alpha) = e^{i\alpha k_{\mathbf{n}}} \tag{A71}$$

with the following.

$$k_{\mathbf{n}} = \zeta_0 (n_1^2 - n_2^2); \qquad \zeta_0 = \frac{\pi^2}{L^2} \frac{1}{4} \sqrt{\frac{5}{\pi}}. \tag{A72}$$

We, thus, have states $|\psi_{n_1 n_2}\rangle$ spanning representation $k_{\mathbf{n}}$. It is, thus, convenient to label the states according to this representation in the following form $|\psi^{k_{\mathbf{n}}}_{n_1 n_2}\rangle$ in such a manner that the following is the case.

$$\hat{U}(\alpha)|\psi^{k_{\mathbf{n}}}_{n_1 n_2}\rangle = e^{i\alpha k_{\mathbf{n}}}|\psi^{k_{\mathbf{n}}}_{n_1 n_2}\rangle. \tag{A73}$$

For the sake of convenience, we introduce the following definitions.

$$k_1 = k_{n_1 n_2} = \zeta_0(n_1^2 - n_2^2); \quad k_2 = k_{n_2 n_1} = \zeta_0(n_2^2 - n_1^2) = -k_1. \tag{A74}$$

Hence, the two-dimensional space (A69) is a representation space spanning the diagonal irreps of the subgroup $\mathcal{T}$.

$$\mathbf{D}^{(k)}(\alpha) = \begin{pmatrix} e^{i\alpha k_1} & 0 \\ 0 & e^{i\alpha k_2} \end{pmatrix} \tag{A75}$$

On the other hand, it is clear that for $n_1 = n_2 = n$, we have a one-dimensional space $\mathcal{L}_1 = \{|\psi_{nn}^{k_0}\rangle\}$ spanning representation $\mathbf{D}^{(k_0)}(\alpha) = 1$ with $k_0 = 0$.

$$\hat{U}(\alpha)|\psi_{nn}^{k_0}\rangle = \mathbf{D}^{(k_0)}(\alpha)|\psi_{nn}^{k_0}\rangle = |\psi_{nn}^{k_0}\rangle. \tag{A76}$$

Once we count on the irreps of subgroup $\mathcal{T}$, we are ready to proceed to construct the irreps of the group $\mathcal{G}$. However, to accomplish this task, it is necessary to recall the concept of conjugate representation.

Let $H \subset G$, with H invariant. Given $\mathbf{D}^{(\mu)}(h)$, the μ-th irrep of $h \in H$, the matrix $\mathbf{D}^{(\mu)}(ghg^{-1}) \equiv {}_{\mu}\mathbf{D}^{(g)}(h)$ called *conjugate representation* is also a representation of H. In our case, $H \to \mathcal{T}$ is an invariant subgroup with representations $D^{(k_\mathbf{n})}(\alpha) = e^{i\alpha k_\mathbf{n}}$. We, thus, have to identify the conjugate representation. In order to achieve this goal, consider the representation k_1 defined by the following.

$$\hat{U}(\alpha)|\psi_{n_1 n_2}^{k_1}\rangle = e^{i\alpha k_1}|\psi_{n_1 n_2}^{k_1}\rangle. \tag{A77}$$

From (A64), we have the following.

$$\mathcal{O}_R \hat{U}(\alpha)\mathcal{O}_R^{-1} = U(\alpha'); \qquad \alpha' = \alpha\chi^{B_1}(R). \tag{A78}$$

Hence, we have the following for the conjugate representation.

$${}_{k_1}D^{(R)}(\alpha) = D^{(k_1)}(\alpha'). \tag{A79}$$

This result can be reinterpreted in the following form:

$${}_{k_1}D^{(R)}(\alpha) = e^{i\alpha\hat{R}\hat{F}^{(B_1)}\hat{R}^{-1}} = e^{i\alpha\chi^{B_1}(R)\hat{F}^{(B_1)}} = e^{i\alpha k'} = D^{(k')}(\alpha), \tag{A80}$$

where the following is the case:

$$k' = k_1\chi^{B_1}(R), \tag{A81}$$

with the proviso that the operators involved act over state $|\psi_{n_1 n_2}^{k_1}\rangle$. Here, we have used simplified notation, $\mathcal{O}_R = \hat{R}$. In addition, it is worth noticing that the following is the case:

$$\langle\psi_{n_1 n_2}^{k_1}|\hat{R}\hat{F}^{(B_1)}\hat{R}^{-1}|\psi_{n_1 n_2}^{k_1}\rangle = \langle\hat{R}^{-1}\psi_{n_1 n_2}^{k_1}|\hat{F}^{(B_1)}|\hat{R}^{-1}\psi_{n_1 n_2}^{k_1}\rangle, \tag{A82}$$

which means that the state spanning the conjugate representation k' is obtained by the following.

$$\hat{R}^{-1}|\psi_{n_1 n_2}^{k_1}\rangle = |\psi_{n_1' n_2'}^{k'}\rangle. \tag{A83}$$

We notice that two irreps are identified, namely k_1 and k_2. Starting with k_1, we obtain conjugate representations ${}_{k_1}D^{(R)}(\alpha) = D^{(k_1)}(RU(\alpha)R^{-1})$, $\forall R \in \mathcal{C}_{4v}$, although some of them are equivalent. The set of nonequivalent representations, denoted by ${}_{k_1}\mathcal{S}$, is called the star of k_1. In our case, from (A81), only two nonequivalent representations are obtained: k_1

itself and $k' = k_2 = -k_1$, the latter generated with $R \in \mathcal{C}_{4v}$ in (A81) satisfying $\chi^{B_1}(R) = -1$. The star is then given by the following:

$$_k\mathcal{S} = {}_{k_1}\mathcal{S} = \{k_1, k_2\}, \tag{A84}$$

where each element is called the prong of the star. Starting with k_2, the same star is obtained. This explains that the star will be referred as ${}_k\mathcal{S}$ without specifying the particular k_i from which it is generated. It should be clear that $|\mathcal{C}_{4v}| = 8$ conjugations are carried out to obtain (A84) of order $|{}_k\mathcal{S}| = 2$. Consequently, there should be a set of elements that transform k_1 to either an equivalent or identical representation. Indeed this set of elements corresponds to the elements of $\mathcal{T}$ as well as the elements of subgroup $\mathcal{C}_{2v}$. This set of transformation form a group, the *little group* of k_1, denoted by $K(k)$ and is given by the following.

$$K(k) = \mathcal{T} \wedge \mathcal{C}_{2v}. \tag{A85}$$

Each prong in star (A84) has associated its own little group, but they are isomorphic, a fact that explains the notation of $K(k)$. The little group of k is infinite. To deal with a finite group, we consider the factor group called *little co-group* $\mathcal{K}(k)$:

$$\mathcal{K}(k) = \frac{K(k)}{\mathcal{T}} \approx \mathcal{C}_{2v}. \tag{A86}$$

in which its elements are provided by the left cosets in the following expansion.

$$K(k) = \sum_{\lambda}^{|\lambda|} s_\lambda \mathcal{T}; \qquad s_\lambda \in \mathcal{C}_{2v}. \tag{A87}$$

On the other hand, the factor group is isomorphic to group $\mathcal{C}_{4v}$:

$$\frac{\mathcal{G}}{\mathcal{T}} \approx \mathcal{C}_{4v}, \tag{A88}$$

with the following expansion in left cosets:

$$\mathcal{C}_{4v} = \sum_{\lambda}^{|\lambda|} p_\lambda \mathcal{C}_{2v}; \qquad |\lambda| = \frac{|\mathcal{C}_{4v}|}{|\mathcal{C}_{2v}|}, \tag{A89}$$

a fact that allows confrontation with finite groups. This is the basic background in the construction of the irreps of $\mathcal{G}$. Expansion (A89) implies that every element $g \in \mathcal{C}_{4v}$ can be expressed in terms of a product of the following form:

$$g = p_\lambda \, h; \quad h \in \mathcal{C}_{2v}, \tag{A90}$$

and in the following explicit form:

$$\mathcal{C}_{4v} = \mathcal{C}_{2v} + \sigma_d^a \mathcal{C}_{2v}, \tag{A91}$$

with identification $p_1 = E, p_2 = \sigma_d^a$.

Let us now consider the ket $|\psi^{k_1}_{n_1 n_2}\rangle$. All the elements of $\mathcal{C}_{2v}$ leave it invariant. On the other hand the action of the coset representatives in the expansion (A89) yields

$$\mathcal{O}_E |\psi^{k_1}_{n_1 n_2}\rangle = |\psi^{k_1}_{n_1 n_2}\rangle, \tag{A92}$$

$$\mathcal{O}_{\sigma_d^a} |\psi^{k_1}_{n_1 n_2}\rangle = |\psi^{k_2}_{n_2 n_1}\rangle. \tag{A93}$$

Hence, the set of functions $\{|\psi^{k_1}_{n_1 n_2}\rangle, |\psi^{k_2}_{n_2 n_1}\rangle\}$ form a representation space of $\mathcal{G}$. However, for the construction of irreps, it is convenient to consider the basis in the following

form: $\{\hat{p}_\lambda|\psi^{k_1}_{n_1n_2}\rangle;\lambda=1,2\}$. The procedure to obtain the irreps of element $g\in\mathcal{C}_{4v}$ consists in applying operator $\hat{g}$ over the representation space. In this manner, we obtain the following:

$$\hat{g}\hat{p}_\lambda|\psi^{k_1}_{n_1n_2}\rangle=\hat{p}_\mu\hat{h}|\psi^{k_1}_{n_1n_2}\rangle;\quad h\in\mathcal{C}_{2v}, \tag{A94}$$

where identity follows from expansion (A89). Here, h is called the sub-element of g in p_λ denoted by $h_\lambda(g)$. All sub-elements involved are listed in Table A3. We should remark that the action over states $|\psi^{k_1}_{n_1n_2}\rangle$ are well defined since they carry irreps of $\mathcal{C}_{2v}$.

Table A3. Sub-elements $h_\lambda(g)$ defined in (A94) through expansion (A89).

g	p_λ	$p_\lambda h$	$h_\lambda(g)$
E	E	E E	E
C_4	E	$\sigma^a_d\sigma^a_v$	σ^a_v
C^3_4	E	$\sigma^a_d\sigma^b_v$	σ^b_v
σ^a_v	E	$E\sigma^a_v$	σ^a_v
σ^b_v	E	$E\sigma^b_v$	σ^b_v
σ^a_d	E	σ^a_dE	E
σ^b_d	E	$\sigma^a_dC_2$	C_2
E	σ^a_d	σ^a_dE	E
C_4	σ^a_d	$E\sigma^b_v$	σ^b_v
C^3_4	σ^a_d	$E\sigma^a_v$	σ^a_v
σ^a_v	σ^a_d	$\sigma^a_d\sigma^b_v$	σ^b_v
σ^b_v	σ^a_d	$\sigma^a_d\sigma^a_v$	σ^a_v
σ^a_d	σ^a_d	EE	E
σ^b_d	σ^a_d	EC_2	C_2

We are now prepared to carry out the induction. However, before we accomplish this goal, it is convenient to present the general procedure. Let us consider the general situation of generating representations of a group G from the irreps $\mathbf{D}^{(\mu)}={}^\mu H$ of $H\subset G$ [10]. First, we expand group G in cosets of H.

$$G=\sum_\lambda^{|\lambda|}s_\lambda H;\quad |\lambda|=\frac{|G|}{|H|}. \tag{A95}$$

The set of cosets $\{s_\lambda H\}$ span a representation of G:

$$\hat{g}(s_\lambda H)=\sum_{\lambda'}^{|\lambda|}\Delta^{(b)}_H(g)_{\lambda'\lambda}\ (s_{\lambda'}H), \tag{A96}$$

where $\Delta^{(b)}(g)$ is called the basal representation given by the following.

$$\Delta^{(b)}_H(g)_{\lambda'\lambda}=\delta_{\lambda'\tau};\qquad gs_\lambda=s_\tau h_\lambda(g). \tag{A97}$$

Let us now consider a set of kets $|\phi^{(\mu)}_i\rangle$ spanning the μ-th irrep ${}_\mu H=\mathbf{D}^{(\mu)}(H)$ of subgroup H.

$$\hat{\mathcal{O}}_R|\phi^{(\mu)}_i\rangle=\sum_j^{n_\mu}D^{(\mu)}_{ji}(R)|\phi^{(\mu)}_j\rangle. \tag{A98}$$

Hence, set $\{\hat{s}_\lambda|\phi^{(\mu)}_i\rangle\}$ is a representation the space of group G:

$$\hat{g}(\hat{s}_\lambda|\phi^{(\mu)}_i\rangle)=\sum_{\lambda'}\sum_j\Delta^{({}_\mu H\uparrow G)}(g)_{\lambda' j;\lambda i}(\hat{s}'_\lambda|\phi^{(\mu)}_j\rangle) \tag{A99}$$

where $\Delta^{(^{\mu}H\uparrow G)}(g)$ is called the induced representation with the following elements.

$$\Delta^{(^{\mu}H\uparrow G)}(g)_{\lambda' j;\lambda i} = \Delta_H^{(b)}(g)_{\lambda'\lambda} D_{ji}^{(\mu)}(h_\lambda(g)). \tag{A100}$$

In general, the induced representation is reducible. However, when induction is carried out through the *little co-groups* associated with the irreps of the subgroup, the induced representations are complete and irreducible. We may, thus, sketch the general procedure as follows. In the frame work of our group $\mathcal{G} = \mathcal{T} \wedge \mathcal{C}_{4v}$, we begin these states, $|\psi_{n_1 n_2}^{k_1}\rangle$, by carrying irreps of the invariant subgroup $\mathcal{T}$. Then, the *little group* $\mathcal{K}(k)$ is identified. This group in infinite; consequently, to deal with a finite group, it is considered the *little co-group* isomorphic to a subgroup of point group $\mathcal{C}_{4v}$. The states $|\psi_{n_1 n_2}^{k_1}\rangle$ span irreps Γ of the *little co-group*, a fact that permits a labeling scheme, $|\psi_{n_1 n_2}^{k_1;\Gamma,\gamma}\rangle$. Finally, induction is carried out by obtaining all irreducible representations of $\mathcal{G}$.

$$\overset{\Gamma,\gamma}{k_1}\mathcal{G} = ^{\Gamma,\gamma} \mathcal{K}(^{k_1}\mathcal{T}) \uparrow \mathcal{G}. \tag{A101}$$

Here, there are two labels, the prong corresponding to the irrep $^{k_1}\mathcal{T}$, and the irrep and component $\{\Gamma, \gamma\}$ associated with the *little co-group*.

We now proceed to generate irreps (A101). In our previous analysis, we were dealing with two-dimensional space (A69) leading to the star (A84), which may be identified with vectors $\{k_1, k_2 = -k_1\}$, as shown in Figure A2. In this figure, we denote $k = k_1$ in accordance with the notation for the *little co-group*. Each prong of the two dimensional star is called a general vector with *little co-group* $\mathcal{C}_{2v}$. On the other hand, the irrep $^{k_0}\mathcal{T}$ spanned by the kets $|\psi_{nn}^{k_0}\rangle$ leads to the star $\mathcal{S}_0 = \{k = 0\}$. Because this irrep $k_0 = 0$ is invariant under full point group $\mathcal{C}_{4v}$, it is called a special point.

Figure A2. Irreducible representations of the group $\mathcal{T}$ labeled by the corresponding little co-groups. Two little co-groups have been identified: $\mathcal{K}(k)$ corresponding to a general vector and $\mathcal{K}(k_0)$ corresponding to special point $k_0 = 0$.

We start considering general points associated with the star (A84). Since in this case the *co-group* is $\mathcal{C}_{2v}$, states $\{|\psi_{n_1 n_2}^{k_1}\rangle, |\psi_{n_2 n_1}^{k_2}\rangle\}$ by itself carry irreps of $\mathcal{C}_{2v}$. Indeed, considering the generators $\{C_2, \sigma_v^a\}$ of the little co-group $\mathcal{C}_{2v}$, we obtain diagonal representations.

$$\Delta(C_2) = \begin{pmatrix} (-1)^{n_1+n_2} & 0 \\ 0 & (-1)^{n_1+n_2} \end{pmatrix}; \quad \Delta(\sigma_v^a) = \begin{pmatrix} (-1)^{n_2+1} & 0 \\ 0 & (-1)^{n_1+1} \end{pmatrix}. \tag{A102}$$

This representation is of course reducible and contains the two irreps given by the following:

$$\mu: \quad D^{(\mu)}(C_2) = (-1)^{n_1+n_2}; \quad D^{(\mu)}(\sigma_v^a) = (-1)^{n_2+1}; \tag{A103}$$

$$\nu: \quad D^{(\nu)}(C_2) = (-1)^{n_1+n_2}; \quad D^{(\nu)}(\sigma_v^a) = (-1)^{n_1+1}, \tag{A104}$$

which have to be identified with the irreps of the $\mathcal{C}_{2v}$ group in accordance to the character in Table A4. Since the little co-groups for k_1 and k_2 are isomorphic, it is enough to consider the reduction associated with k_1, which is displayed in Table A5.

Table A4. Character table for group $\mathcal{C}_{2v}$.

$\mathcal{C}_{2v}$	E	C_2	$\sigma_v(xz)$	$\sigma_v(yz)$		
A_1	1	1	1	1	z	$x^2; y^2; z^2$
A_2	1	1	-1	-1	R_z	xy
B_1	1	-1	1	-1	$x; R_y$	xz
B_2	1	-1	-1	1	$y; R_x$	yz

Table A5. Identification of the irreps of $\mathcal{C}_{2v}$ in accordance with parity.

	$n_1 = 2m+1$ $n_2 = 2n+1$	$n_1 = 2m$ $n_2 = 2n$	$n_1 = 2m$ $n_2 = 2n+1$	$n_1 = 2m+1$ $n_2 = 2n$
$D^{(\mu)}(C_2)$	1	1	-1	-1
$D^{(\mu)}(\sigma_v^a)$	1	-1	1	-1
$k_1 : \mu$	A_1	A_2	B_1	B_2

We proceed to obtain the representations of $\mathcal{G}$ that are completely specified by the matrix representation of generators $\{U(\alpha), C_4, \sigma_d^a\}$. Let us start considering element $g = C_4$. In accordance with the coset expansion (A89), the representation space is $\{E|\psi^{k_1}\rangle, \sigma_d^a|\psi^{k_1}\rangle\}$. From Table A3 for the sub-elements, we obtain the following:

$$C_4[E|\psi^{k_1,\mu}\rangle] = \sigma_d^a\sigma_v^a|\psi^{k_1,\mu}\rangle = \chi^{(\mu)}(\sigma_v^a)[\sigma_d^a|\psi^{k_1,\mu}\rangle], \tag{A105}$$

$$C_4[\sigma_d^a|\psi^{k_1,\mu}\rangle] = E\sigma_v^b|\psi^{k_1,\mu}\rangle = \chi^{(\mu)}(\sigma_v^b)[E|\psi^{k_1,\mu}\rangle], \tag{A106}$$

from which we obtain the matrix representation for element C_4.

$$\mathbf{D}^{({}^{\mu}_{k}\mathcal{G})}(C_4) = \begin{pmatrix} 0 & \chi^{(\mu)}(\sigma_v^b) \\ \chi^{(\mu)}(\sigma_v^a) & 0 \end{pmatrix}. \tag{A107}$$

In similar manner for element σ_d^a, we have the following:

$$\sigma_d^a[E|\psi^{k_1,\mu}\rangle] = \chi^{(\mu)}(E)[\sigma_d^a|\psi^{k_1,\mu}\rangle], \tag{A108}$$

$$\sigma_d^a[\sigma_d^a|\psi^{k_1,\mu}\rangle] = \chi^{(\mu)}(E)[E|\psi^{k_1,\mu}\rangle], \tag{A109}$$

and, consequently, we have the following.

$$\mathbf{D}^{({}^{\mu}_{k}\mathcal{G})}(\sigma_d^a) = \begin{pmatrix} 0 & \chi^{(\mu)}(E) \\ \chi^{(\mu)}(E) & 0 \end{pmatrix}. \tag{A110}$$

Finally, we have to obtain the matrix representation of element $U(\alpha)$. The action of an element of $\mathcal{T}$ over an element of the basis is given by the following:

$$\hat{U}(\alpha)\hat{R}|\psi_{n_1n_2}^{k_1,\mu}\rangle = \hat{R}\hat{U}(\alpha')|\psi_{n_1n_2}^{k_1,\mu}\rangle; \quad R = E, \sigma_d^a. \tag{A111}$$

where we have taken into account the invariance of $\mathcal{T}$. Nevertheless, from (A83), the new element $U(\alpha')$ is associated with the inverse of R.

$$\hat{U}(\alpha')|\psi_{n_1n_2}^{k_1,\mu}\rangle = {}_{k_1}D^{(R^{-1})}(\alpha)|\psi_{n_1n_2}^{k_1,\mu}\rangle = e^{i\alpha k'}|\psi_{n_1n_2}^{k_1,\mu}\rangle. \tag{A112}$$

However, in this case, $R^{-1} = R$ and, consequently, the following is the case.

$$\mathbf{D}^{({}^{\mu}_{k}\mathcal{G})}(\alpha) = \begin{pmatrix} e^{i\alpha k} & 0 \\ 0 & e^{-i\alpha k} \end{pmatrix}. \tag{A113}$$

We now consider the special point $k_0 = 0$. In this case, the little co-group is $\mathcal{C}_{4v}$ and the basal representation is generated by element $E\mathcal{C}_{4v}$ with basis $|\psi_{nn}^{k_0,\mu}\rangle$. The action of the generators is as follows.

$$\hat{U}(\alpha) = 1, \tag{A114}$$

$$\hat{C}_4(E|\psi_{nn}^{k_0,\mu}\rangle) = (-1)^{n+1}(E|\psi_{nn}^{k_0,\mu}\rangle), \tag{A115}$$

$$\hat{\sigma}_d^a(E|\psi_{nn}^{k_0,\mu}\rangle) = (E|\psi_{nn}^{k_0,\mu}\rangle). \tag{A116}$$

From the character in Table A2, we have identifications for the following representations:

$$n \quad \text{even} \quad D^{(^{B_2}_{k_0}\mathcal{G})}(C_4) = -1; \quad D^{(^{B_2}_{k_0}\mathcal{G})}(\sigma_d^a) = 1; \tag{A117}$$

$$n \quad \text{odd} \quad D^{(^{A_1}_{k_0}\mathcal{G})}(C_4) = 1; \quad D^{(^{A_1}_{k_0}\mathcal{G})}(\sigma_d^a) = 1, \tag{A118}$$

and in compact form in terms of characters.

$$D^{(^{\mu}_{k_0}\mathcal{G})}(\alpha) = 1; \tag{A119}$$

$$D^{(^{\mu}_{k_0}\mathcal{G})}(C_4) = \chi^{(\mu)}(C_4); \quad ; D^{(^{\mu}_{k_0}\mathcal{G})}(\sigma_d^a) = \chi^{(\mu)}(\sigma_d^a). \tag{A120}$$

Finally, we present subduction ${}^{\mu}_{k}\mathcal{G} \downarrow \mathcal{C}_{4v}$ in order to make clear that the accidental degeneracy previously identified in $\mathcal{C}_{4v}$ renders a natural degeneracy in group $\mathcal{G}$. In Table A6, we present subduction ${}^{\mu}_{k}\mathcal{G} \downarrow \mathcal{C}_{4v}$ where we can observe that the accidental degeneracy in accordance with geometrical group $\mathcal{C}_{4v}$ is indeed a natural degeneracy in the new symmetry group, $\mathcal{G}$.

Table A6. Subduction ${}^{\mu}_{k}\mathcal{G} \downarrow \mathcal{C}_{4v}$.

$\mathcal{C}_{4v}$	E	C_4, C_4^3	C_4^2	σ_v^a, σ_v^b	σ_d^a, σ_d^b	${}^{\mu}_{k}\mathcal{G} \downarrow \mathcal{C}_{4v}$
$\chi^{(^{A_1}_{k_o}\mathcal{G})}$	1	1	1	1	1	A_1
$\chi^{(^{B_2}_{k_o}\mathcal{G})}$	1	-1	1	-1	1	B_2
$\chi^{(^{A_1}_{k}\mathcal{G})}$	2	0	2	2	0	$A_1 \oplus B_1$
$\chi^{(^{A_2}_{k}\mathcal{G})}$	2	0	2	-2	0	$A_2 \oplus B_2$
$\chi^{(^{B_1}_{k}\mathcal{G})}$	2	0	-2	0	0	E
$\chi^{(^{B_2}_{k}\mathcal{G})}$	2	0	-2	0	0	E

Remark A1. *In the construction of irreps of space groups, an induction process is followed from the irreps of the translational group to the space group. The procedure we have presented has a close analogy with space groups. Our group $\mathcal{T}$ corresponds to the translational group while irreps k corresponds to the momentum space involved in the Bloch functions. This is the reason we have used the language of solid state physics to developed the representation theory of the new group, $\mathcal{T} \wedge \mathcal{C}_{4v}$.*

References

1. Cohen-Tannoudji, C.; Diu, B.; Laloë, F. *Quantum Mechanics*; John Wiley and Sons: New York, NY, USA, 1977; Volume I.
2. Levin, F.S. *An Introduction to Quantum Theory*; Cambridge University Press: Cambridge, UK, 2002.
3. Greiner, W. *Quantum Mechanics. An Introduction*; Springer: Frankfurt am Main, Germany, 1989.
4. Harris, D.; Bertolucci, M.D. *Symmetry and Spectroscopy. An Introduction to Vibrational and Electronic Spectroscopy*; Dover Publications, Inc.: New York, NY, USA, 1989.
5. MacIntosh, H. *Symmetry and Degeneracy. Group Theory and Its Application*; Loebel, E.M., Ed.; Academic Press: New York, NY, USA, 1971; Volume 2, pp. 75–144.
6. Wybourne, B. *Classical Groups for Physicists*; Wyley: New York, NY, USA, 1974.

7. Fock, V. Zur Theorie des Wasserstoffatoms. *Z. Phys.* **1935**, *98*, 145. [CrossRef]
8. Bargmann, V. Zur Theorie des Wasserstoffatoms. *Z. Phys.* **1936**, *99*, 576. [CrossRef]
9. Leybraz F.; Frank, A.; Lemus, R.; Andrés, M.V. Accidental degeneracy in a simple quantum system: A new symmetry group for a particle in an impenetrable square-well potential. *Am. J. Phys.* **1997**, *65*, 1087. [CrossRef]
10. Altmann, S.L. *Induced Representations in Crystals and Molecules. Point, Space and Non-Rigid Molecular Groups*; Academic: New York, NY, USA, 1977.
11. Hernández-Castillo, A.O.; Lemus, R. Symmetry group of an impenetrable cubic well potential. *J. Phys. A Math. Theor.* **2013**, *46*, 465201. [CrossRef]
12. Lemus, R.; Frank, A.; Andrés, M.V.; Leybraz, F. Accidental degeneracy and hidden symmetry: Rectangular wells with commensurate sides. *Am. J. Phys.* **1998**, *66*, 629. [CrossRef]
13. Harris, D.O.; Engerholm, G.G.; Gwinn, W.D. Calculation of Matrix Elements for One-Dimensional Quantum-Mechanical Problems and the Application to Anharmonic Oscillators. *J. Chem. Phys.* **1965**, *43*, 1515. [CrossRef]
14. Dickinson, A.S.; Certain, P.R. Calculation of Matrix Elements for One-Dimensional Quantum-Mechanical Problems. *J. Chem. Phys.* **1968**, *49*, 4209. [CrossRef]
15. Lill, J.V.; Parker, G.A.; Light, J.C. Discrete variable representations and sudden models in quantum scattering theory. *Chem. Phys. Lett.* **1982**, *89*, 483. [CrossRef]
16. Light, J.C.; Hamilton, I.P.; Lill, J.V. Generalized discrete variable approximation in quantum mechanics. *J. Chem. Phys.* **1985**, *82*, 1400. [CrossRef]
17. Baĉić, Z.; Light, J.C. Highly excited vibrational levels of "floppy" triatomic molecules: A discrete variable representation—Distributed Gaussian basis approach. *J. Chem. Phys.* **1986**, *85*, 4594. [CrossRef]
18. Lill, J.V.; Parker, G.A.; Light, J.C. The discrete variable–finite basis approach to quantum scattering *J. Chem. Phys.* **1986**, *85*, 900. [CrossRef]
19. Light, J.C.; Baĉić, Z. Adiabatic approximation and nonadiabatic corrections in the discrete variable representation: Highly excited vibrational states of triatomic molecules. *J. Chem. Phys.* **1987**, *87*, 4008. [CrossRef]
20. Baĉić, Z.; Light, J.C. Accurate localized and delocalized vibrational states of HCN/HNC. *J. Chem. Phys.* **1987**, *86*, 3065. [CrossRef]
21. Choi, S.E.; Light, J.C. Use of the discrete variable representation in the quantum dynamics by a wave packet propagation: Predissociation of $NaI(^1\Sigma_0^+) \rightarrow NaI(0^+) \rightarrow Na(^2S)+I(^2P)$. *J. Chem. Phys.* **1989**, *90*, 2593. [CrossRef]
22. Tennison, J. Highly excited rovibrational states using a discrete variable representation: The H_3^+ molecular ion. *J. Chem. Phys.* **1989**, *91*, 3815. [CrossRef]
23. Light, J.C.; Carrington, T., Jr. Discrete-Variable Representations and their Utilization In *Advances in Chemical Physics*; Prigogine, I., Rice, S.A., Eds.; John Wiley & Sons: Hoboken, NJ, USA, 2000; Volume 114, p. 263.
24. Shizgal, B.D.; Blackmore, R. A discrete ordinate method of solution of linear boundary value and eigenvalue problems. *J. Comput. Phys.* **1984**, *55*, 313. [CrossRef]
25. Shizgal, B.D.; Chen, H. The quadrature discretization method (QDM) in the solution of the Schrödinger equation with nonclassical basis functions. *J. Chem. Phys.* **1996**, *104*, 4137. [CrossRef]
26. Shizgal, B.D. *Spectral Methods in Chemistry and Physics. Applications to Kinetic Theory and Quantum Mechanics*; Springer: New York, NY, USA, 2015.
27. Shizgal, B.D. Pseudospectral method of solution of the Schrödinger equation with non classical polynomials; the Morse and Pöschl–Teller (SUSY) potentials. *Comp. Theor. Chem.* **2016**, *1084*, 51. [CrossRef]
28. Shizgal, B.D. A comparison of pseudospectral methods for the solution of the Schrödinger equation; the Lennard-Jones (n, 6) potential. *Comp. Theor. Chem.* **2017**, *1114*, 25. [CrossRef]
29. Bao, J.; Shizgal, B.D. Pseudospectral method of solution of the Schrödinger equation for the Kratzer and pseudoharmonic potentials with nonclassical polynomials and applications to realistic diatom potentials. *Comp. Theor. Chem.* **2019**, *1149*, 49. [CrossRef]
30. Baye, D.; Heenen, P.H. Generalised meshes for quantum mechanical problems. *J. Phys. A Math. Gen.* **1986**, *19*, 2041. [CrossRef]
31. Vincke, M.; Malegat, L.; Baye, D. Regularization of singularities in Lagrange-mesh calculations. *J. Phys. B At. Mol. Opt. Phys.* **1993**, *26*, 811. [CrossRef]
32. Baye, D. Lagrange-mesh method for quantum-mechanical problems. *Phys. Stat. Sol.* **2006**, *243*, 1095. [CrossRef]
33. Baye, D. The Lagrange-mesh method. *Phys. Rep.* **2015**, *565*, 1. [CrossRef]
34. Carvajal, M.; Arias, J.M.; Gómez-Camacho, J. Configuration localized Morse wave functions: Application to vibrational transitions in anharmonic diatomic molecules. *Phys. Rev. A* **1999**, *59*, 1852. [CrossRef]
35. Carvajal, M.; Arias, J.M.; Gómez-Camacho, J. Analytic evaluation of Franck-Condon integrals for anharmonic vibrational wave functions. *Phys. Rev. A* **1999**, *59*, 3462. [CrossRef]
36. Pérez-Bernal, F.; Arias, J.M.; Carvajal, M.; Gómez-Camacho, J. Configuration localized wave functions: General formalism and applications to vibrational spectroscopy of diatomic molecules. *Phys. Rev. A* **2000**, *61*, 042504. [CrossRef]
37. Wei, H.; Carrington, T. The discrete variable representation of a triatomic Hamiltonian in bond length–bond angle coordinates. *J. Chem. Phys.* **1992**, *97*, 3029. [CrossRef]
38. Wang, X.-G.; Carrington, T. A discrete variable representation method for studying the rovibrational quantum dynamics of molecules with more than three atoms. *J. Chem. Phys.* **2009**, *130*, 094101. [CrossRef]

39. Bramley, M.J.; Carrington, T. A general discrete variable method to calculate vibrational energy levels of three- and four-atom molecules. *J. Chem. Phys.* **1993**, *99*, 8519. [CrossRef]
40. Bramley, M.J.; Tromp, J.W.; Carrington, T.; Corey, G.C. Efficient calculation of highly excited vibrational energy levels of floppy molecules: The band origins of H_3^+ up to 35 000 cm^{-1}. *J. Chem. Phys.* **1994**, *100*, 6175. [CrossRef]
41. Wang, X.-G.; Carrington, T. The Utility of Constraining Basis Function Indices When Using the Lanczos Algorithm to Calculate Vibrational Energy Levels. *J. Phys. Chem. A* **2001**, *105*, 2575. [CrossRef]
42. Iachello, F.; Levine, R.D. *Algebraic Theory of Molecules*; Oxford University Press: Oxford, UK, 1995.
43. Lemus, R. Unitary group approach for effective molecular potentials: 1D systems. *Mol. Phys.* **2019**, *117*, 167. [CrossRef]
44. Lemus, R. A simple approach to solve the time independent Schröedinger equation for 1D systems. *J. Phys. Comm.* **2019**, *3*, 025012. [CrossRef]
45. Estévez-Fregoso, M.M.; Arias, J.M.; Gómez-Camacho, J.; Lemus, R. An approach to establish a connection between algebraic and configuration spaces: $su(\nu+1)$ algebraic model for vibrational excitations. *Mol. Phys.* **2018**, *116*, 2254. [CrossRef]
46. Estévez-Fregoso, M.M.; Lemus, R. Connection between the $su(3)$ algebraic and configuration spaces: Bending modes of linear molecules. *Mol. Phys.* **2018**, *116*, 2374. [CrossRef]
47. Rodríguez-Arcos, M.; Lemus, R. Unitary group approach for effective potentials in 2D systems: Application to carbon suboxide C_3O_2. *Chem. Phys. Lett.* **2018**, *713*, 266. [CrossRef]
48. Rodríguez-Arcos, M.; Lemus, R.; Arias, J.M.; Gómez-Camacho, J. Unitary group approach to describe interatomic potentials in 3D systems. *Mol. Phys.* **2019**, *118*, e1662959. [CrossRef]
49. Rodríguez-Arcos, M.; Bermúdez-Montaña, M.; Arias, J.M.; Gómez-Camacho, J.; Orgaz, E.; Lemus, R. Algebraic discrete variable representation approaches: Application to interatomic effective potentials. *Mol. Phys.* **2021**, *119*, e1876264 . [CrossRef]
50. Bermúdez-Montaña, M.; Rodríguez-Arcos, M.; Lemus, R.; Arias, J.M.; Gómez-Camacho, J.; Orgaz, E. Algebraic DVR Approaches Applied to Describe the Stark Effect. *Symmetry* **2020**, *12*, 1719. [CrossRef]
51. Moshinsky, M. *The Harmonic Oscillator in Modern Physics: From Atoms to Quarks*; Gordon and Breach: New York, NY, USA, 1969.
52. Littlejohn, R.G.; Cargo, M. A general framework for discrete variable representation basis sets. *J. Chem. Phys.* **2002**, *116*, 8691. [CrossRef]
53. Barletta, P.; Lombardi, M.; Kievsky, A. Variational DVR Calculations. *Few-Body Syst.* **2004**, *34*, 11. [CrossRef]
54. Chen, J.-Q. *Group Representation Theory for Physicists*; World Scientific: New York, NY, USA, 1989.
55. Lemus, R. A general method to obtain vibrational symmetry adapted bases in a local scheme. *Mol. Phys.* **2003**, *101*, 2511. [CrossRef]
56. Álvarez-Bajo, O.; Lemus, R.; Carvajal,M.; Pérez-Bernal, F. Equivalent rotations associated with the permutation inversion group revisited: Symmetry projection of the rovibrational functions of methane. *Mol. Phys.* **2011**, *109*, 797. [CrossRef]
57. Lemus, R. Quantum Numbers and the Eigenfunction Approach to Obtain Symmetry Adapted Functions for Discrete Symmetries. *Symmetry* **2012**, *4*, 667. [CrossRef]
58. Bermúdez-Montaña, M.; Lemus, R.; Castaños, O. Fidelity, entropy, and Poincaré sections as tools to study the polyad breaking phenomenon. *EPL* **2016**, *116*, 13001. [CrossRef]
59. Bermúdez-Montaña, M.; Lemus, R.; Castaños, O. Polyad breaking phenomenon associated with a local-to-normal mode transition and suitability to estimate force constants. *Mol. Phys.* **2017**, *115*, 3076. [CrossRef]
60. Pöschl, G.; Teller, E. Bemerkungen zur Quantenmechanik des anharmonischen Oszillators. *Z. Phys.* **1933**, *83*, 143. [CrossRef]
61. Rosen, N.; Morse, P.M. On the Vibrations of Polyatomic Molecules. *Phys. Rev.* **1932**, *42*, 210. [CrossRef]
62. Landau, L.D.; Lifshitz, E.M. *Quantum Mechanics, Non Relativistic Theory*, 3rd ed.; Pergamon: Oxford, UK, 1997.
63. Arias, J.M.; Gómez-Camacho, J.; Lemus, R. An $su(1,1)$ dynamical algebra for the Pöschl–Teller potential. *J. Phys. A Math. Gen.* **2004**, *37*, 877. [CrossRef]
64. Gradshtein, I.S.; Rizhic, I.M. *Tables of Integrals, Series and Product*, 5th ed.; Academic Press: New York, NY, USA, 1994.
65. Morse, P.M. Diatomic Molecules According to the Wave Mechanics. II. Vibrational Levels. *Phys. Rev.* **1929**, *34*, 57. [CrossRef]
66. Matsumoto, A. Generalised matrix elements in discrete and continuum states for the Morse potential. *J. Phys. B: At. Mol. Opt. Phys.* **1988**, *21*, 2863. [CrossRef]
67. Benedict, M.G.; Molnár, B. Algebraic construction of the coherent states of the Morse potential based on supersymmetric quantum mechanics. *Phys. Rev. A* **1999**, *60*, R1737. [CrossRef]
68. Molnar, B.; Földi, P.; Benedict, M.G.; Bartha, F. Time evolution in the Morse potential using supersymmetry: Dissociation of the NO molecule. *EPL* **2003**, *61*, 445. [CrossRef]
69. Lemus, R.; Arias, J.M.; Gómez-Camacho, J. An $su(1,1)$ dynamical algebra for the Morse potential. *J. Phys. A Math. Gen.* **2004**, *37*, 1805. [CrossRef]
70. Bardoni, A.; Manini, N. Systematic calculation of molecular vibrational spectra through a complete Morse expansion. *Int. J. Quantum Chem.* **2007**, *107*, 782. [CrossRef]